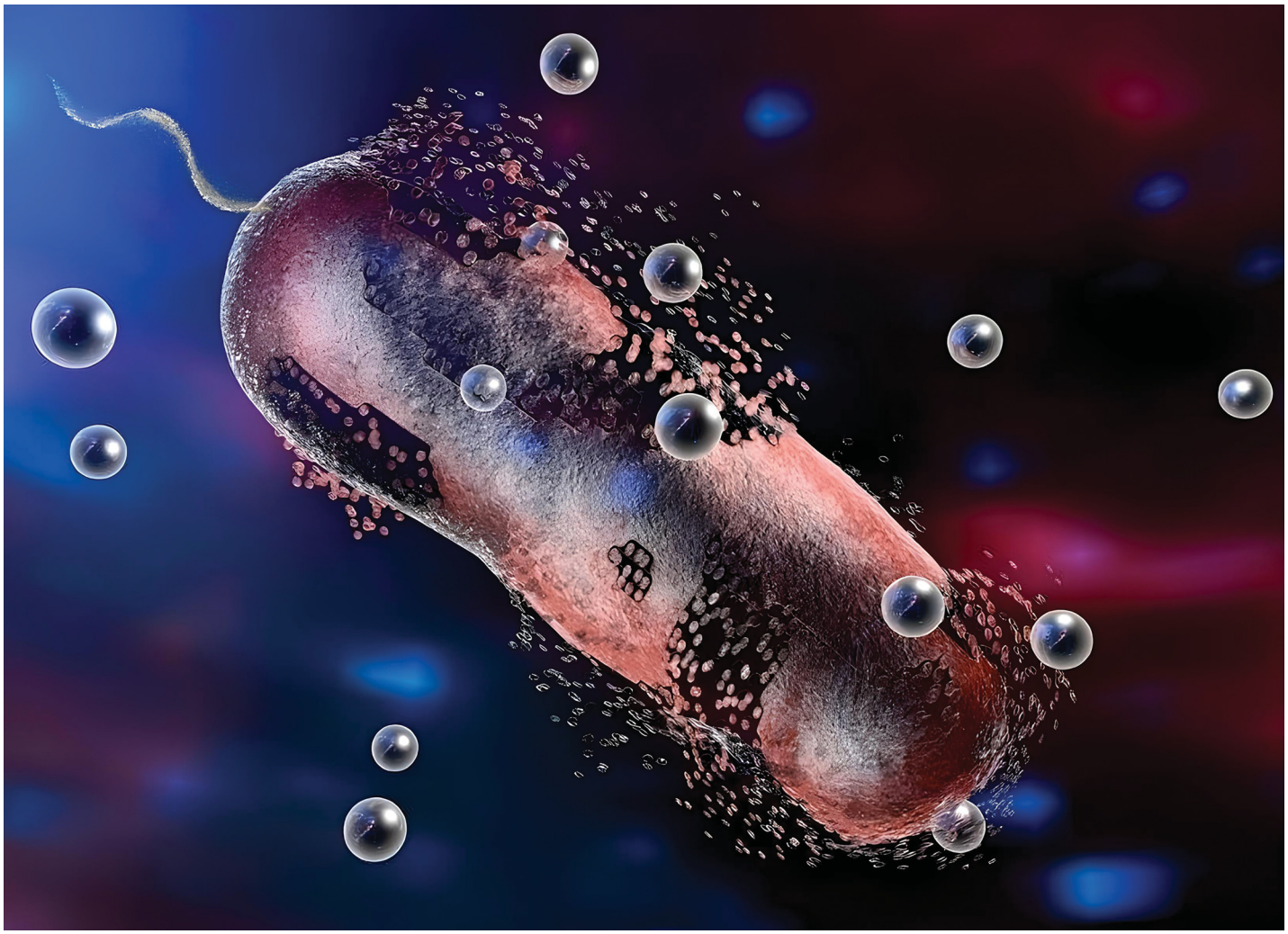

Showcasing research from Professor Shailesh Narain Sharma's laboratory at CSIR- National Physical Laboratory, India, and Dr Rajni Verma's contribution at Seoul National University, South Korea.

Multifaceted properties of TiO_2 nanoparticles synthesized using *Mangifera indica* and *Azadirachta indica* plant extracts: antimicrobial, antioxidant, and non-linear optical activity investigation for sustainable agricultural applications

This research unveils a significant stride in addressing global food scarcity, introducing green synthesized TiO_2 nanoparticles derived from medicinal plant extract. The obtained multifunctional nanoparticles exhibit exceptional antimicrobial efficacy as well as robust non-linear optical properties. The demonstrated antimicrobial activity against various fungi and bacteria, known to impact crop yield, reveals promising applications in agriculture. The Basic Science Research Program through the National Research Foundation of Korea (NRF) funded by the Ministry of Science, ICT & Future Planning (NRF-2021R1A2C2013543) provides support to feature the artwork on the journal cover.

As featured in:

See Rajni Verma, Shailesh Narain Sharma *et al.*, *Mater. Adv.*, 2024, **5**, 2767.

ROYAL SOCIETY OF CHEMISTRY

rsc.li/materials-advances

Registered charity number: 207890

Materials Advances

ROYAL SOCIETY OF CHEMISTRY

PAPER

View Article Online
View Journal | View Issue

Cite this: *Mater. Adv.*, 2024, 5, 2767

Multifaceted properties of TiO_2 nanoparticles synthesized using *Mangifera indica* and *Azadirachta indica* plant extracts: antimicrobial, antioxidant, and non-linear optical activity investigation for sustainable agricultural applications†

Archana Rana,[ab] Saurabh Pathak,[c] Kapil Kumar,[ab] Anjali Kumari,[de] Samridhi Chopra,[ab] Mahesh Kumar,[ab] Deeba Kamil,[e] Ritu Srivastava,[ab] Sang-Koog Kim,[c] Rajni Verma *[c] and Shailesh Narain Sharma *[ab]

The increasing global food scarcity necessitates the development of nanomaterials with low toxicity for use as antimicrobial agents and sensors to mitigate agricultural losses. In this study, we present an investigation into the green synthesis of titanium dioxide nanoparticles (TiO_2 NPs) utilizing plant extracts derived from *Azadirachta indica* (*A. indica*) and *Mangifera indica* (*M. indica*) as reducing and stabilizing agents. The antimicrobial activity of the NPs is investigated against a range of pathogenic fungi (*A. alternata*, *C. gloeosporioides*, *T. harzianum*, and *A. rolfsii*) and a bacterial species (*X. oryzae*) known to significantly impact crop yield in agriculture. Remarkably, the TiO_2 NPs exhibit potent inhibitory action against all tested microorganisms, suppressing their growth over an extended period as revealed by the zone of inhibition (ZOI) estimated *via* disc diffusion assay. This can be attributed to the generation of reactive oxygen species (ROS), including hydroxyl radicals, in close proximity to the microbial cell wall. Furthermore, the free radical scavenging activity was confirmed by a dose-dependent response in the 2,2-diphenyl-1-picrylhydrazyl (DPPH) assay, demonstrating their substantial antioxidant activity. Moreover, we also explore the non-linear optical (NLO) properties of the TiO_2 NPs through Z-scan measurements employing femtosecond (fs) laser pulses. Notably, both types of NPs exhibit reverse saturable absorption (RSA) behaviour when excited by femtosecond laser pulses, enabling the determination of the nonlinear absorption coefficient and nonlinear refractive index through fitting open and closed aperture curves. The calculated values of the nonlinear susceptibility of NPs synthesized using *M. indica* and *A. indica* are $2.43 \times 10^{-15} + i.7.2 \times 10^{-18}$ and $3.91 \times 10^{-15} + i.1.06 \times 10^{-18}$, respectively. These values reflect the robust NLO response of NPs, indicating their potential for a wide range of applications. Combining their potent antimicrobial activity, antioxidant properties, and strong nonlinear optical characteristics, these NPs hold tremendous promise in addressing critical challenges in sustainable agriculture.

Received 14th July 2023,
Accepted 2nd January 2024

DOI: 10.1039/d3ma00414g

rsc.li/materials-advances

1. Introduction

Food security, a critical global concern, pertains to the availability, accessibility, and affordability of food. This issue is amplified by the growing global population and shifting environmental conditions.[1] Particularly, climate change has a severe impact on agriculture and food production, due to more frequent and severe weather events like droughts and floods, which lead to crop failure and food shortage.[2] Moreover, plant diseases caused by various pathogens, including bacteria, viruses, and fungi, can cause significant crop losses and reduce

[a] *CSIR-National Physical Laboratory, Dr K.S. Krishnan Marg, New Delhi 110012, India. E-mail: shailesh@nplindia.org*
[b] *Academy of Scientific and Innovative Research (AcSIR), Ghaziabad, 201002, India*
[c] *National Creative Research Initiative Center for Spin Dynamics and SW Devices, Nanospinics Laboratory, Research Institute of Advanced Materials, Department of Materials Science and Engineering, Seoul National University, Seoul 151-744, South Korea. E-mail: rajni.verma@snu.ac.kr*
[d] *SHUATS- Sam Higginbottom University of Agriculture, Technology, and Sciences, Allahabad, Uttar Pradesh, India*
[e] *IARI-Indian Agricultural Research Institute, Pusa, New Delhi-110012, India*

† Electronic supplementary information (ESI) available. See DOI: https://doi.org/10.1039/d3ma00414g

food quality, exacerbating the challenge of meeting the surging demand for food.[3] Although conventional agricultural practices, like use of chemical pesticides and fungicides, have yielded some success in controlling and detecting diseases, they possess several limitations.[4] These methods can be expensive and have adverse impacts on the environment, leading to resistance development in pathogens over time, reducing their effectiveness. Thus, innovative and sustainable approaches are needed to tackle plant diseases and boost food security.[5,6]

Pathogenic fungi such as *Alternaria alternata* (*A. alternata*), *Colletotrichum gloeosporioides* (*C. gloeosporioides*), and *Athelia rolfsii* (*A. rolfsii*) pose significant threats to agricultural productivity. *A. alternata* is a broad-range pathogen that infects diverse crops, causing diseases such as Alternaria leaf spot, fruit rot, and blight. These diseases have detrimental effects, leading to reduced crop yields, compromised quality, and economic setbacks for farmers.[7] Similarly, *C. gloeosporioides* is notorious for causing anthracnose disease, characterized by sunken lesions, rotting, and fruit drop.[8] The impact of this fungus is severe, causing substantial agricultural losses in terms of yield reduction and decreased market value of affected crops. In addition to these fungi, the bacterial pathogen *Xanthomonas oryzae* (*X. oryzae*) poses a significant threat to rice production. It is responsible for bacterial leaf blight, a devastating disease that affects the leaves of rice plants.[9] This disease manifests as chlorosis, lesions, and, in severe cases, complete crop failure. Bacterial leaf blight has a profound impact on rice production, leading to substantial losses in both yield and quality.[10] To mitigate the adverse effects of these pathogens, farmers must implement effective disease management strategies.[11]

Over the past few decades, nanotechnology has undergone remarkable advancements, leading to enhanced performance of various systems across a wide range of fields such as electronics,[12,13] medicine,[14] energy,[15,16] sensing[17] and materials science,[18] opening up new possibilities and improving the efficiency and functionality of numerous applications.[19] Nanotechnology offers a promising solution to the challenges faced in agriculture, leveraging the unique physical and chemical properties of nanomaterials for various agricultural applications, particularly disease detection and control.[20] Nanoscale materials, with their high surface-to-volume ratios, have the capacity to interact at the molecular level, leading to the development of nanomaterial-based sensors that detect the early signs of plant diseases.[21] Additionally, nanomaterials enable the targeted delivery of fungicides or insecticides directly to infected sites, minimizing chemical usage and non-target organism impact.[22,23] Furthermore, nanotechnology enhances fertilizer efficiency by encapsulating and delivering nutrients to plant roots, reducing nutrient loss and environmental impacts.[24] Nanomaterials can improve food production quality and quantity by controlling the release of pesticides, reducing resistance development in pests and weeds. Safety and environmental concerns require appropriate regulation and analysis of long-term effects of nanomaterials on agriculture.[25]

Among metal oxide nanoparticles, TiO_2 NPs are widely used in agriculture due to their antimicrobial activity against a range of plant pathogens.[26] They show enhanced performance compared to their bulk counterparts, attributed to their small size, large surface area, and high reactivity.[27,28] Their contact with microbial cells leads to increased efficacy, penetrating cell walls and causing membrane damage. Additionally, TiO_2 NPs possess photoactivity, generating ROS upon exposure to light. Due to this property, they effectively target pathogens sensitive to oxidative stress, contributing to their antimicrobial action.[29] Moreover, these NPs exhibit biocompatibility and biodegradability, ensuring environmental safety. TiO_2 NPs also possess unique NLO properties, making them suitable for the development of biosensors.[30] These NLO materials respond to specific stimuli, emitting light at different wavelengths.[31] When incorporated into sensors, NPs enable the detection of changes in temperature and humidity or specific chemicals present in the environment, aiding in monitoring soil moisture, nutrient levels, and pest infestation.[32] Furthermore, NLO properties facilitate imaging and visualization, enabling the detection of plant diseases and the monitoring of crop growth.[33] These properties offer opportunities for developing innovative and sustainable sensing technologies in agriculture. TiO_2 NPs demonstrate a rapid and notably substantial NLO response.[34] This characteristic has led to their utilization in combination with other materials to modify or augment their NLO properties. Trejo-Valdez *et al.* successfully employed TiO_2 NPs alongside Au NPs, showcasing altered or enhanced NLO responses.[35] Additionally, Dong *et al.* achieved an enhanced broadband NLO response through the incorporation of TiO_2 as a dopant in CuO nanosheets.[36] Numerous other studies provide evidence supporting the notion that the introduction of TiO_2 into various materials enhances their NLO response.

TiO_2 NPs can be synthesized through established techniques, including green synthesis, sol–gel, hydrothermal, and precipitation methods.[37] These methods offer a reliable framework for achieving precise control over the size, morphology, and crystalline structure of the NPs.[38] Green synthesis, in particular, aligns with sustainable practices by utilizing plant extracts and natural sources as both reducing and stabilizing agents.[39] However, non-conventional methods, such as microfluidic reactors, microwave-assisted synthesis, and sonochemical synthesis, have gained recognition for their efficiency, speed, and eco-friendliness.[40] Although conventional methods provide a sturdy foundation, non-conventional methods offer promising avenues for innovation and customization.[41] In our study, we prefer conventional methods rooted in the pursuit of well-defined, reproducible results. Nevertheless, given the dynamic landscape of NP synthesis, we anticipate that non-conventional methods will play an increasingly vital role in future investigations and large scale synthesis of NPs for applications. These methods contribute to the continuous evolution of efficient, sustainable, and tailored protocols for NP synthesis.[42]

Green synthesis has emerged as a preferable method for producing NPs due to its environmentally friendly nature and sustainability.[43] Unlike traditional chemical synthesis, green synthesis utilizes natural sources, such as plant extracts, to

produce NPs without the need for toxic solvents or reducing agents.[44] This method minimizes environmental impacts, generates no toxic waste, and relies on renewable resources.[45] Recently, Ansari *et al.* synthesized TiO_2 NPs using the *Acorus calamus* leaf extract to probe their antimicrobial activity against Gram-positive and Gram-negative bacteria.[46] They have reported excellent antimicrobial activity of green synthesized NPs against the selected Gram-positive bacteria (*B. subtilis* and *S. aureus*) over Gram-negative pathogenic bacteria (*P. aeruginosa* and *E. coli)*. Achudhan *et al.* synthesized TiO_2 NPs from the natural extracts of *Azadirachta indica* twigs, *Ficus benghalensis*, and *Syzygium aromaticum* and reported their significant antibacterial and antifungal properties, inhibiting the formation of biofilms of *Streptococcus mutans*, *Citrobacter freundii*, and *Candida albicans.*[47] They also demonstrated larvicidal activity against the Zika virus vector *Aedes aegypti*, with a mortality rate of 98% at a concentration of 75 μg mL^{-1}. The properties of NPs derived from various plant extracts vary due to the unique phytochemical composition present in each extract.[48] It is crucial to conduct comprehensive studies to thoroughly examine the physicochemical attributes of these NPs. Such investigations are essential for optimizing their performance and harnessing their full potential in diverse applications.[49]

The present study is focused on the synthesis of TiO_2 NPs using leaf extracts from *M. indica* and *A. indica* plants. The primary objective is to investigate the NLO properties of the NPs through the Z-scan method. Additionally, we aim to evaluate the NPs' potential as an antimicrobial agent targeting plant pathogens, particularly bacteria and fungi that adversely impact agricultural crops. This dual focus on NLO and antimicrobial properties aligns with the overarching goal of sustainable agriculture. Specifically, the NPs are examined for their effectiveness against prevalent plant pathogens, including *A. alternata*, *A. rolfsii*, *C. gloeosporioides*, *T. harzianum*, and *X. oryzae*. The envisaged outcome is a comprehensive understanding of the NPs' capabilities both as disease detection sensors and as agents, combatting microbial threats in agriculture. By synthesizing TiO_2 NPs *via* an environmentally friendly means, utilizing plant extracts, and subjecting them to rigorous assessment of their antimicrobial activities and NLO properties, this study aims to contribute significantly to the progress of eco-friendly nanotechnology in the agricultural domain. Such advancements have the potential to minimize crop losses and increase overall agricultural productivity.

2. Experimental methods and materials

2.1. Chemicals and pathogens

Titanium(IV) isopropoxide (TTIP), sodium hydroxide, ethanol and streptomycin sulphate were acquired from Sigma-Aldrich for the synthesis. The synthesis was performed using Millipore DI water. Agar powder and dextrose anhydrous were purchased from Srichem Consultants Private Limited, Hyderabad, India. Different fungi such as *Alternaria alternata* (*A. alternata*), *Colletotrichum gloeosporioides* (*C. gloeosporioides*), *Trichoderma harzianum* (*T. harzianum*), and *Athelia rolfsii* (*A. rolfsii*) and the bacterial pathogen *Xanthomonas Oryzae* (*X. oryzae*) were collected from IARI, New Delhi.

2.2. Preparation of *M. indica* and *A. indica* plant leaf extracts

The leaves of *M. indica* and *A. indica* were gathered from the medicinal plant farm of the National Physical Laboratory, New Delhi, India. The collected leaf samples were surface cleaned with running faucet water to eliminate soil followed by washing with DI water thrice. The obtained leaves were shade dried for a few days at room temperature. The dried samples were powdered in a mortar pestle to get a uniform size range. Then 10 g of *M. indica* and *A. indica* powdered leaf samples were mixed in 200 ml of DI water boiled at 70–80 °C for 30 min. The resulting solution was then filtered using Whatman no. 1 filter paper and subsequently stored at 4 °C for NP synthesis. The filtrate was utilized for the synthesis of NPs.

2.3. Preliminary phytochemical screening:

Preliminary chemical reactions were performed to test the presence of various metabolites in both the plant extracts.[50] The brief procedure of the chemical test is described in Section S1 (ESI†). It was observed that both *A. indica* and *M. indica* plant extracts possessed the metabolites shown in Table 1.

It is important to note that the concentration of each metabolite may differ in both the plant extracts. The exact concentration of each metabolite is not known.

2.4. Green synthesis of TiO_2 NPs

TiO_2 NPs were synthesized using *A. indica* and *M. indica* leaf extracts, following previously reported procedures with slight modifications.[46] The leaf extracts act as both the capping and reducing agents, while TTIP served as the precursor for producing TiO_2 NPs. Firstly, 4 ml of TTIP was dissolved in 50 ml of leaf extract, stirred and heated for 2 hours at 80 °C. During the reaction, the colour change was observed from a light green and white solidified precursor to an orange colour over time. The particles were observed to be mixed and dissolved completely in the extract for 2 hours. After that the resulting slurry was collected in Petri dishes and dried overnight at 60 °C. The dried powder was then crushed with a mortar and pestle and annealed in a furnace at 400 °C for 2 hours, which transformed the orange-coloured powder to white powder. The resulting

Table 1 Different metabolites present in the plant extracts

	Metabolites	
Functional groups	*M. indica*	*A. indica*
Flavonoids	+	+
Steroids	+	+
Terpenoids	+	+
Phenols	+	+
Saponins	+	+
Proteins	+	+

TiO_2 NPs were used for further experiments without further modification.

2.5. Materials characterization

The structural, morphological, optical, and antimicrobial properties of the prepared NPs were characterized using various analytical techniques. The crystalline structure and crystallite size of TiO_2 NPs were determined using X-ray diffraction (XRD) analysis on a Rigaku Miniflex-II instrument with CuKα radiation (λ = 1.540 Å) in the 2θ range of 10–80°.[51] The morphology and particle size distribution of the NPs were determined by scanning electron microscopy (SEM) and transmission electron microscopy (TEM) using a ZEISS instrument and an FEI Philips Morgagni 268D instrument, respectively. The UV-visible absorbance spectra of the NPs were recorded using a Shimadzu UV-3101 spectrophotometer in the range of 200–800 nm.[52,53] The functional groups present in the NPs were analysed by Fourier transform infrared (FTIR) spectroscopy using a Perkin-Elmer BX-II spectrophotometer within the wave-number range of 4000–400 cm^{-1}.[54] The specific surface area and pore size of the NPs were measured using the Brunauer–Emmett–Teller (BET) NOVA instrument *via* nitrogen adsorption–desorption studies conducted at 77 K. Furthermore, the third-order NLO properties, such as non-linear absorption, refractive index and susceptibility, of the 0.05 mg ml^{-1} NP suspension were determined by a conventional Z-scan measurement employing a Ti:sapphire pulsed laser source (Legend USP and Coherent Micra) of wavelength 800 nm with a repetition rate and a pulse width of 1 kHz and 35–45 fs, respectively.[55] The Z-scan setup was calibrated using CS_2 solvent, ensuring accurate measurement for linearly plane-polarized incident light in the visible spectrum.

2.6. Antimicrobial activity determined by disk diffusion assay

The antimicrobial action of the synthesized NPs was evaluated against the fungal pathogens of *A. alternata*, *C. gloeosporioides*, *T. harzianum*, and *A. rolfsii* and the bacterial pathogen of *X. oryzae.* The disk diffusion method was adopted to monitor the antimicrobial activity of synthesized NPs as reported by Degado *et al.*[56] The microbial strains were collected from the Indian Agricultural Research Institute (IARI), Pusa, India. The strains were refreshed in an 8.5 cm Petri dish containing potato-dextrose agar (PDA) at 37 °C for 7 days. PDA broth was prepared using 10 g of agar powder, 10 g of dextrose anhydrous, potato extracts (100 ml), and DI water (400 ml). Flasks were autoclaved at 115 °C for 3 h in a dark environment.

To produce fungal biomass for determining TiO_2 NP antifungal activity, a small number of fresh mycelia were harvested from the plates and transferred to a 500 ml flask containing PDA broth.[57] 10 ml of fungus-containing PDA is added into different Petri dishes to rest and it is allowed to solidify. Specific fungal pathogens were inoculated in PDA medium along with the antibiotic streptomycin sulphate to prevent contamination (2 g). 5 mm (diameter) discs were prepared using a sterile filter paper (disc cutter) on the potato-dextrose agar broth solution that carried pathogens. Different concentrations of TiO_2 NPs prepared using different plant extracts (60, 80 and 100 μg ml^{-1}) were added to the discs; simultaneously, deionized water was used as a positive control. The inoculated cultured plates were incubated at 37 °C for 48 h, and the diameter of the zone of inhibition (ZOI) was measured in mm, and the findings were recorded throughout studies.

The antibacterial activity of TiO_2 NPs was tested against *X. oryzae* bacterial strain inoculated on the plate using the disk diffusion method performed as described previously by Perez *et al.* with minor changes.[58] The nutrient agar medium was separately placed in Petri dishes, and 10 μl of a bacterial culture with a concentration of 10^7 CFU ml^{-1} was spread on the Petri dishes with a spreader and allowed to settle overnight. Different TiO_2 NP concentrations (60, 80 and 100 μg ml^{-1}) were added to various Petri dishes with deionized water, which is also used as a control, and incubated at 30 °C for 48 h. The antibacterial activity was determined by measuring the ZOI. There were duplicates for each treatment of NPs for both fungi and bacteria with the same concentration.

2.7. Estimation of antioxidant efficacy by DPPH free radical scavenging assay

DPPH is a stable synthetic-free radical widely used to investigate the free radical scavenging activity of natural products or synthetic compounds. The antioxidant activities of TiO_2 NPs synthesized using two plant extracts were determined at different concentrations (50, 100, 150, 200, 300, 350, and 400 μg ml^{-1}) using DPPH assay. In brief, 3 ml of 0.1 mM DPPH solution was prepared in 50% methanol (working solution), along with different concentrations of the TiO_2 NPs and ascorbic acid (control sample).[59] This reaction mixture was incubated for 30 min at room temperature under dark conditions. The absorbances of the test and standard reaction mixtures were obtained at 517 nm. Radical scavenging activity was calculated using the following formula:[60]

$$\text{DPPH radical scavenging activity}(\%) = \left[\frac{(\text{absorbance})_{\text{control}} - (\text{absorbance})_{\text{sample}}}{(\text{absorbance})_{\text{control}}}\right] \times 100$$

3. Results and discussion

3.1. Phase identification and crystal structure

The XRD spectra were obtained for TiO_2 NPs synthesized using *A. indica* and *M. indica*, in the 2θ range of 10–80°, using an X-ray diffractometer at a wavelength of 1.5406 Å.[61] TiO_2 NPs can exist in anatase, rutile, brookite, and amorphous phases, depending on various factors such as synthesis conditions, temperature, and pressure. Anatase is formed at low temperatures, high pH, and low precursor concentration, while rutile is favoured at high temperatures, low pH, and high precursor concentration.[28] Brookite is formed under hydrothermal or solvothermal conditions with specific additives, and the amorphous phase can be obtained through non-equilibrium processes like

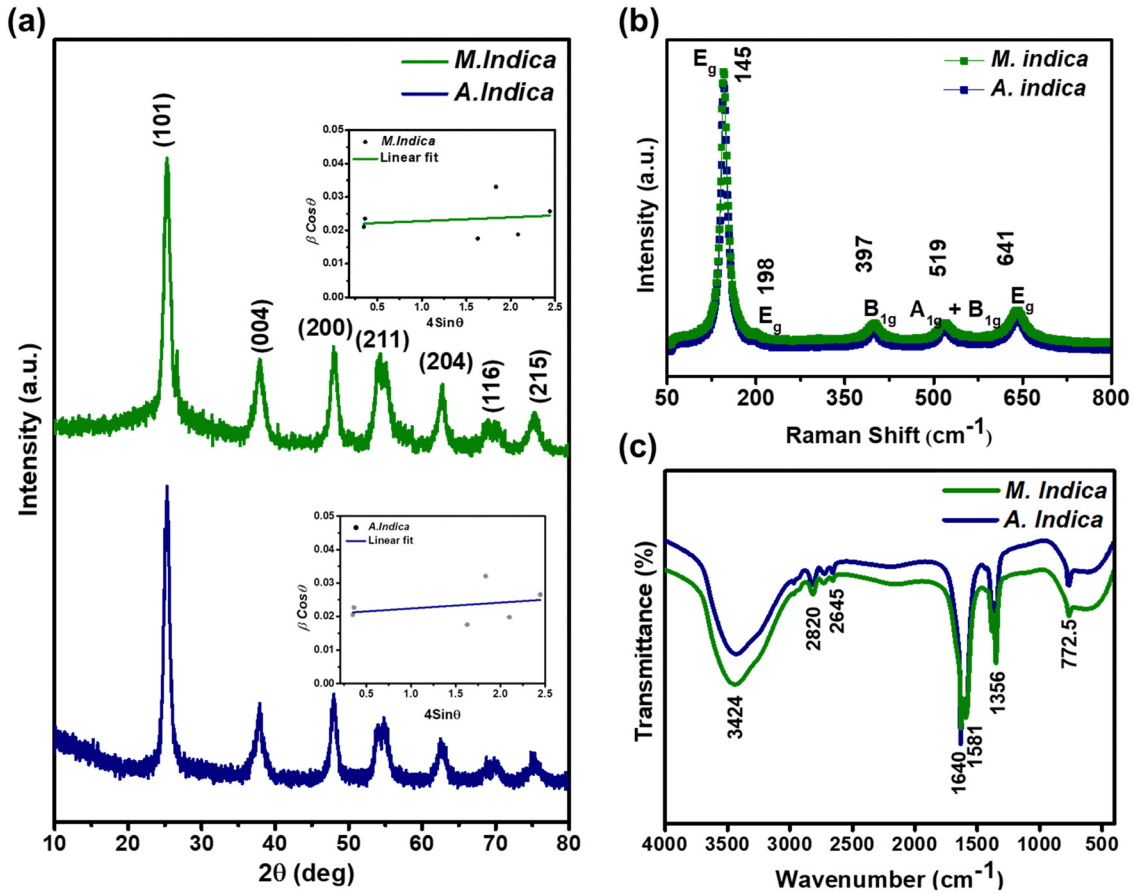

Fig. 1 (a) XRD patterns, (b) Raman spectra and (c) FTIR spectra of green synthesized TiO_2 NPs obtained using *A. indica* and *M. indica* plant extracts. The insets of (a) display the corresponding Williamson–Hall plots.

sol–gel, precipitation, or combustion synthesis. Precursor concentration, pH, and the presence of dopants or surfactants also influence phase formation.[62] The XRD patterns of the TiO_2 NPs synthesised using *A. indica* and *M. indica* are shown in Fig. 1(a). The diffraction peaks at the 2θ values of 25.19°, 38.02°, 47.93°, 54.62°, 62.72°, 69.06° and 75.75° correspond to diffraction planes (101), (004), (200), (211), (204), (116), and (215), which confirm the anatase phase (JCPDS no. 89-4921) of the *A. indica* derived NP sample.[63] The TiO_2 NPs synthesized using *M. indica* also show diffraction peaks in close proximity to those of the TiO_2 NPs synthesized using *A. indica*. The TiO_2 NPs synthesized using *A. indica* have lattice parameters of $a = b =$ 3.778 Å and $c = 9.509$ Å, while those synthesized using *M. indica* have lattice parameters of $a = b = 3.789$ Å and $c = 9.521$ Å. It is important to note that the standard lattice parameter values of TiO_2 are $a = b = 3.784$ Å and $c = 9.515$ Å. The (101) plane exhibits the highest peaks, and the other planes are comparatively broader, indicating a smaller crystallite size.[62] Furthermore, the crystallite sizes of both NP samples were determined using Scherrer's equation,[64] which is expressed as $D = \frac{0.9\lambda}{\beta_{hkl}\cos\theta}$, where D is the crystallite size in nanometers, β_{hkl} is the full-width at half-maximum, θ is the Bragg's angle of reflection, and λ is the wavelength of X-ray (= 1.54 Å).[65] The crystallite sizes of TiO_2 NPs synthesized using *A. indica* and *M. indica* were calculated to be 11.2 nm and 11.9 nm, respectively.[66] However, the determination of the crystallite size through Scherrer's equation is susceptible to peak broadening effects.[67] Consequently, for a more accurate calculation of the crystallite size, we have employed the Williamson–Hall method by fitting a straight line using equation:[68] $\beta_{hkl}\cos\theta = 4\varepsilon\sin\theta + \frac{k\lambda}{D}$ where ε is the lattice strain and k is the shape factor.[54] The Williamson–Hall plot for both NP samples is shown in the inset of Fig. 1(a). The crystallite size and lattice strain obtained for the TiO_2 NPs prepared using *A. indica* are 9.3 nm and 0.0036, respectively, while for the TiO_2 NPs prepared using *M. indica*, the values are 10.1 nm and 0.0039, respectively.[69]

The Raman spectra of both the TiO_2 NPs exhibited characteristic peaks at 145 (E_g), 198 (E_g), 397 (B_{1g}), 519 ($A_{1g} + B_{1g}$), and 641 (E_g) cm^{-1} (Fig. 1(b)), which were consistent with the anatase phase of TiO_2. The peak observed at 145 cm^{-1} corresponds to the E_g mode and is related to the symmetric stretching vibration of Ti–O bonds.[70] The peak observed at 198 cm^{-1} also corresponds to the E_g mode and is related to the symmetric bending vibration of Ti–O bonds. The peak observed at 397 cm^{-1} corresponds to the B_{1g} mode and is related to the anti-symmetric bending vibration of O–Ti–O bonds.[71] The peak

observed at 519 cm^{-1} corresponds to the $A_{1g} + B_{1g}$ mode and is related to the mixed mode of symmetric stretching and anti-symmetric bending vibrations of O–Ti–O bonds. The peak observed at 641 cm^{-1} corresponds to the E_g mode and is related to the bending vibration of Ti–O–Ti bonds.[71] These Raman peaks are associated with the vibrational modes of the TiO_2 lattice structure, and their positions and intensities provide information about the crystal phase, particle size, and defects in the material.[70] The presence of these characteristic peaks at specific wavelengths confirms the anatase phase of TiO_2 NPs and provides insights into their structural properties.

The FTIR spectra of both TiO_2 NP samples are shown in Fig. 1(c), which demonstrate the characteristics of the formation of high purity products revealing the presence of various functional groups in the samples. A broad band observed in between 3600 and 3000 cm^{-1}, *i.e.* 3424 cm^{-1}, is related to the O–H stretching mode of the hydroxyl group, indicating the presence of moisture in the sample. The peak at 1640 cm^{-1} is associated with the O–H bending mode of adsorbed water molecules.[52] The broad band from 1000–400 cm^{-1} corresponds to Ti–O stretching and Ti–O–Ti bridging stretching modes. It has been reported that the peak in the range of 800–400 cm^{-1} is the contribution from the anatase phase of TiO_2 NPs.[72] Thus, the characteristic peak at 772.5 cm^{-1} confirms the formation of the anatase phase of NPs, attributed to the stretching vibration of Ti–O–Ti linkage.[52] The obtained product can show weak absorption bands corresponding to the residual organic species that have not been completely removed during the reaction process.[52] The organic impurities could be hydroxyl, carboxylate and alkane groups, which have not been washed off with ethanol and distilled water. Two weak bands at 2645 and 2820 cm^{-1} are assigned to the C–H stretching vibrations of alkane groups. The peaks at 1356 and 1581 cm^{-1} could be attributed to carboxyl and methylene groups, which has also resulted from the residual organic species.

3.2. Morphology and size distribution

The fine-scale topological features of the samples were evaluated using SEM analysis. The SEM micrographs in Fig. 2(a) and (b) depict the slightly agglomerated spherical-like morphology of the NPs synthesized using *A. indica* and *M. indica* plant extracts, respectively. The agglomeration was observed throughout the region of NPs synthesized using *M. indica* (Fig. 2(a)), whereas less agglomeration was noticed in NPs synthesized using *A. indica* (Fig. 2(b)). These variations may be attributed to several factors: (i) the presence of different phytochemicals such as polyphenols, flavonoids, terpenoids, and alkaloids in both the plant extracts, leading to various interactions with metal precursors and affecting the nucleation and growth of NPs, (ii) the different compounds within the extracts possessing diverse abilities to reduce metal ions and stabilize NPs, resulting in size variation, and (iii) the variation in the types and nature of antioxidants present in the plant extracts, which can influence the reduction reaction of the metal precursor during NP synthesis.[73] Further insights into the morphology were obtained through TEM analysis (Fig. 2(c) and (d)). The bright field TEM images of both the samples revealed agglomeration in the NPs synthesized using *M. indica* (Fig. 2(c)), whereas the NPs synthesized using *A. indica* (Fig. 2(d)) showed less agglomeration, which is consistent with the SEM analysis. This suggests that the NPs synthesized using *A. indica* act as a better capping agent compared to *M. indica.* The particle sizes of the NPs were determined through fitting the particle size distribution plot, revealing size ranges of approximately 8–28 nm for those produced using *M. indica* and 3–27 nm for those produced using *A. indica* (Fig. S1, ESI†).[67] Notably, the majority of NPs in both cases exhibited a median size of 20 nm. The average particle sizes of NPs synthesized using *M. indica* and *A. indica* were measured as 18.9 nm and 19.6 nm, respectively. Moreover, Fig. 2(e) presents the high-resolution transmission electron microscopy (HRTEM) image of the TiO_2 NPs synthesized using *M. indica.* The image reveals a distinct lattice spacing of 0.237 nm, corresponding to the (004) plane of the anatase phase. Furthermore, the polycrystalline nature of the sample is evident in Fig. 2(f), where multiple bright fringes are observed. Notably, lattice planes, specifically (101) and (004), are clearly identifiable in the selected area electron diffraction (SAED) pattern. The elemental composition of Ti and O in NPs prepared using *A. indica* and *M. indica* plant extracts were confirmed using EDX, as shown in Table S1 (ESI†).

To gain a deeper understanding of the mechanism, the surface properties of the NPs were examined through BET characterization. Fig. 2(g) and (h) display the nitrogen adsorption–desorption isotherms of NPs obtained using both plant extracts. The volume adsorbed *vs.* relative pressure curve corresponds to a type IV adsorption isotherm with an H4 hysteresis curve and mesoporous phases, according to the IUPAC classification.[74] The presence of a type IV hysteresis loop indicates the existence of mesoporous materials with a narrow pore size distribution. Furthermore, the Barrett–Joyner–Halenda (BJH) model (inset of Fig. 2(g) and (h)) was employed to calculate the average pore diameter and volume of the green-synthesized NP samples.[74] The surface areas of TiO_2 NPs synthesized using *A. indica* and *M. indica* were determined to be 94.09 $m^2\ g^{-1}$ and 127.60 $m^2\ g^{-1}$, respectively. The average pore diameters were calculated to be 4.1 nm and 5.8 nm, while the average pore volumes were found to be 1.307 cc g^{-1} and 1.205 cc g^{-1} for TiO_2 NPs produced using *A. indica* and *M. indica* plant extracts. The higher pore diameter directly corresponds to enhanced antimicrobial activity, as discussed in the further section on antimicrobial activity.

3.3. Linear and nonlinear optical properties of TiO_2 NPs determined using UV-vis spectroscopy, PL spectroscopy and Z-scan measurements

The optical properties of the NPs were investigated through UV-vis and PL spectroscopy measurements. UV-visible light ranging from 200 to 600 nm was employed to evaluate the light absorption characteristics of TiO_2 NPs. Fig. 3 illustrates the UV-visible spectra of TiO_2 NPs synthesized using *A. indica* and *M. indica* plant extracts in an aqueous solution at room temperature. The absorption maxima (λ_{max}) were observed at

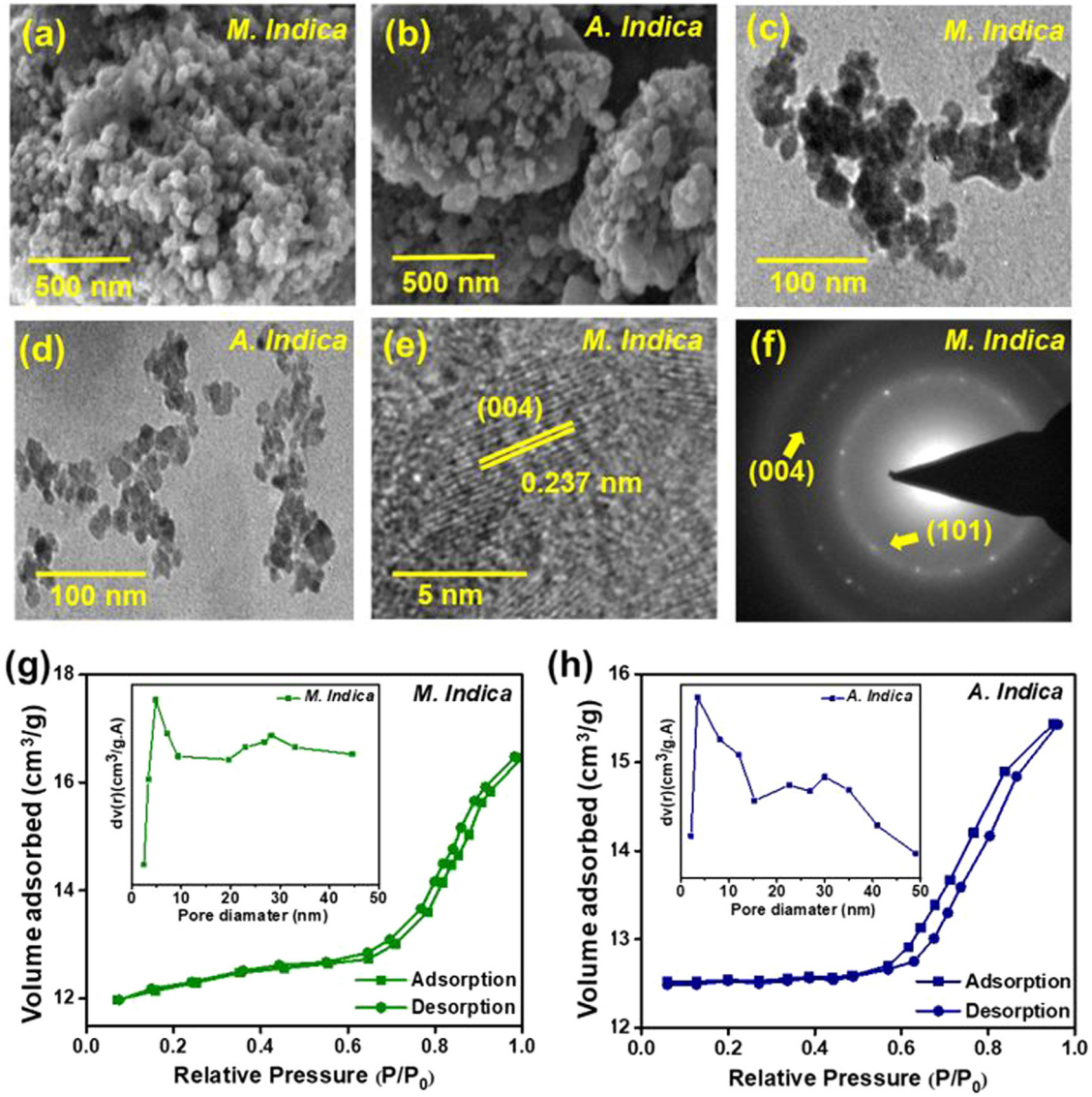

Fig. 2 (a) and (b) SEM micrographs, (c) and (d) TEM images of the TiO_2 NPs prepared using *M. indica* and *A. indica* plant extracts, respectively. (e) HRTEM image and (f) SAED pattern of the TiO_2 NPs prepared using *M. indica*. (g) and (h) N_2 adsorption–desorption isotherm plots of the TiO_2 nanoparticles. Insets in (g) and (h) illustrate the pore size distributions obtained from the BJH desorption pore volume data of the respective samples.

337 nm and 341 nm for the NPs synthesized using *M. indica* and *A. indica*, respectively. Although there was a very slight difference, the absorption maxima were found to be similar. This minor variation could be attributed to differences in the particle size of the NPs synthesized using the two different plant extracts.[75] The optical bandgap (E_g) of the green-synthesized NP samples was determined using a Tauc plot, $h\nu$ *versus* $(\alpha h\nu)^2$, as shown in the inset of Fig. 3, and the following equation:[76] $(ah\nu)^{\frac{1}{n}} = k(h\nu - E_g)$, where k is a constant, $h\nu$ is the photon energy, E_g is the band gap, and α is the absorption coefficient.[53] The values of n are $\frac{1}{2}$ and 2 for indirect and direct band gaps, respectively, depending on the nature of the electronic transition. The bandgap energies of the two types of TiO_2 NPs synthesized using *M. indica* and *A. indica* were estimated to be 2.9 eV and 3.1 eV, respectively. These values correspond to the electronic transition from the valence band to the conduction band (O-2p and Ti-3d).[28] Furthermore, the photoluminescence spectra provide insights into exciton recombination and surface defects. Fig. 3(b) presents the PL spectra of TiO_2 NPs synthesized using *M. indica* and *A. indica* plant extracts at an excitation wavelength of 370 nm. The emission peaks were observed at 455 nm and 470 nm, exhibiting equal intensities. These emissions at 455 nm and 470 nm are attributed to surface state emissions, resulting from the recombination of trapped electron–hole pairs arising from dangling bonds in the NPs.[26] The similar intensities of both peaks suggest that there is no significant variation in the particle size between the NPs prepared using the two different plant extracts.

The NLO properties of the nanoscale materials are ideal for the development of a variety of applications including, optical switching and modulation, laser, signal processing and

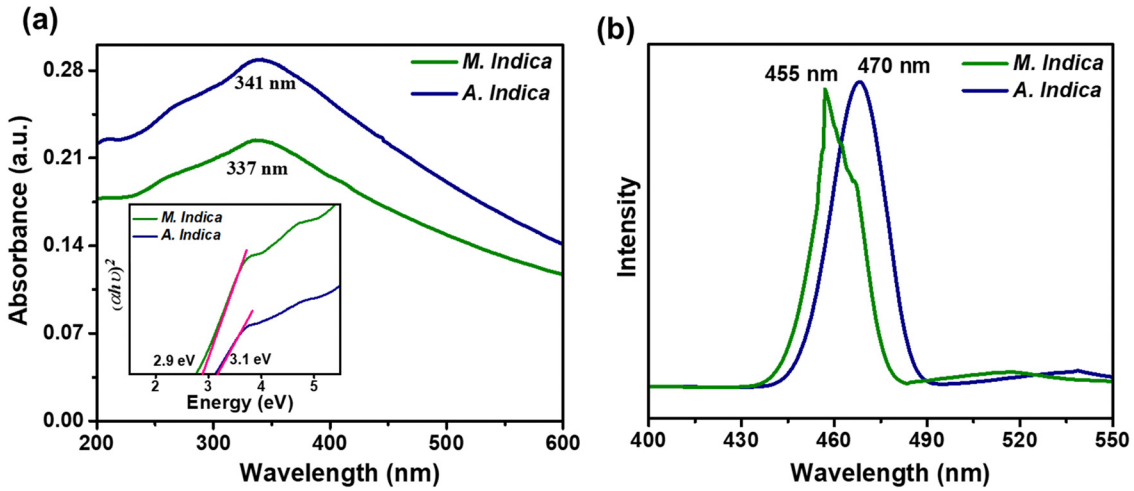

Fig. 3 (a) Ultraviolet-visible absorption spectra and (b) photoluminescence spectra obtained at an excitation wavelength of 370 nm for TiO_2 NPs synthesized using *M. indica* and *A. indica* plant extracts. The inset in (a) displays the Tauc plot illustrating the band gap energy values.

bioimaging.[77] Nanomaterial-based biosensors with NLO properties have the potential to revolutionize agriculture by providing rapid, sensitive, label-free, and portable detection methods for various analytes.[78] They enable real-time monitoring, precision agriculture, and environmental sustainability, thereby contributing to improved crop quality, yield, and resource management in agricultural applications. We have probed the NLO parameters of the TiO_2 NPs using Z-scan measurement, *i.e.*, the nonlinear absorption coefficient (β) and refractive index (n_2) are measured to calculate the third-order nonlinear susceptibility.[55]

Fig. 4 illustrates the schematic representation of the Z-scan setup employed for determining various NLO parameters. The Z-scan measurement of TiO_2 NPs was conducted using a 35 fs Ti:sapphire pulsed laser system consisting of the Legend USP and Coherent Micra lasers, operating at a wavelength (λ) of 800 nm. To generate mode-locked Gaussian-shaped pulses, a repetition rate of 1 kHz and a pulse width of 35–45 fs were employed. The laser beam was split into two components using beam splitters. One component served as the pump, passing through an operational parametric amplifier (OPA), while the other component was directed towards the spectrometer after passing through a delay stage.[55] The probe beam, known as the white light continuum (WLC), was generated by a sapphire disc and transmitted through the delay stage. The open and closed curves were determined using the Z-scan setup and a linear translator.[79] The experimental results were obtained for both open and closed apertures of TiO_2 NPs at a concentration of 0.05 mg ml^{-1}. The laser beam was focused onto the TiO_2 NPs using a convex lens with a beam waist of 40 μm and a focal length of 40 cm. The sonicated NPs were placed in a 1 mm quartz cuvette for observation. The nonlinear parameters, such as the absorption coefficient and refractive index, were measured to calculate the third-order nonlinear susceptibility.

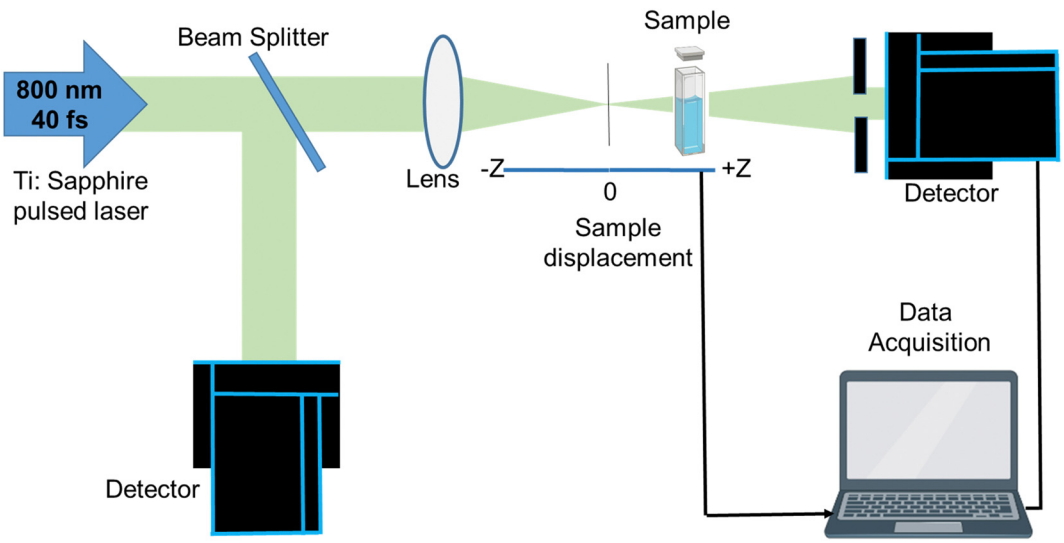

Fig. 4 Schematic of the Z-scan measurement setup used for probing the nonlinear optical properties of TiO_2 NPs.[79]

The closed aperture Z-scan technique was used to determine the nonlinear refractive index, while the open aperture technique involved unlocking the aperture before the detector to measure two-photon absorption (2PA) and nonlinear absorption.[79]

Third-order NLO processes can be categorized into resonant and nonresonant types. Resonant processes involve actual electronic transitions and exhibit relatively slow response times, typically in the nanosecond range.[80] In contrast, nonresonant processes involve virtual transitions and display faster response times, often in the picosecond or femtosecond range. Resonant nonlinearities encompass phenomena like saturable absorption (SA), RSA, excited state absorption (ESA), free carrier absorption (FCA), nonlinear refraction (NLR), and nonlinear scattering (NLS).[81] Nonresonant nonlinearities, on the other hand, include two-photon absorption and multiphoton absorption (MPA), which occur when multiple photons are absorbed simultaneously.[82] It is important to acknowledge that resonant nonlinearities primarily depend on the total energy of the incident pulse, while nonresonant nonlinearities, such as 2PA and MPA, rely on the maximum intensity of the incident light. TiO_2 NPs can exhibit RSA or SA depending on the experimental conditions and the specific characteristics of the NPs. In the case of pure TiO_2 NPs, they typically display RSA behaviour.[83] RSA occurs when the absorption of light increases with increasing light intensity. This phenomenon arises due to a combination of NLO effects, such as 2PA and excited-state absorption ESA. In RSA, at low light intensities, the NPs are in the ground state and have low absorption. However, as the intensity increases, 2PA and ESA processes become more significant, leading to a nonlinear increase in absorption. It is important to note that the behaviour of TiO_2 nanoparticles, including RSA or SA, can also depend on other factors such as particle size, surface modifications, excitation wavelength, and experimental conditions.[82]

The results obtained from the open and closed aperture Z-scan measurements of the TiO_2 NPs are shown in Fig. 5(a)–(d), where the symbols represent the experimental data and the solid lines represent theoretical fitting. It is noteworthy that the corresponding measurement curve exhibits a well-defined peak of the normalized transmittance. This distinctive peak is indicative of the presence of RSA in both samples, whereby the absorption of light by the material diminishes as the intensity of the incident light increases. Open aperture Z-scan measures laser beam transmission through the sample, providing insights

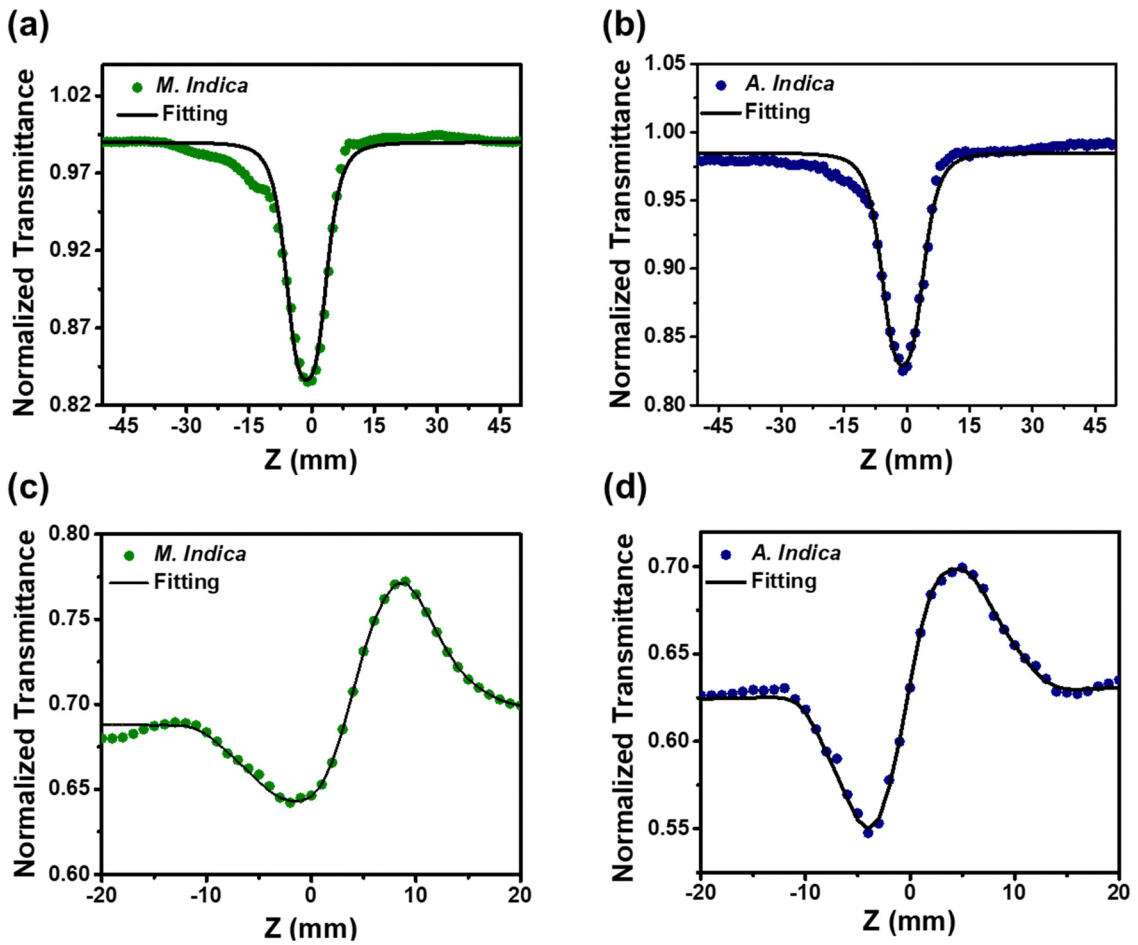

Fig. 5 (a) and (b) Open aperture and (c) and (d) close aperture Z-scan measurements of TiO_2 NPs at 35 fs laser excitation. Closed symbols are the experimental data, while the solid lines are theoretical fits.

into both nonlinear absorption and refraction. Closed aperture Z-scan, using an aperture, measures transmitted intensity as the sample is moved, primarily capturing nonlinear refraction effects.[79] Under the experimental conditions employed in our study, it is not feasible to induce a direct electronic transition from the ground state to the excited state through one-photon absorption. This limitation arises due to the energy of the excitation light (1.55 eV) being insufficient to bridge the energy gap (E_g) between the two states. Consequently, the only viable pathway for electrons to reach the excited state is through MPA. Interestingly, the band gap energy values obtained from our UV-vis spectroscopy analysis, ranging from 2.9 to 3.1 eV, align closely with the energy requirements for 2PA. Therefore, it is highly likely that 2PA serves as the dominant absorption mechanism in our experimental system. Furthermore, the values of the nonlinear absorption coefficient were calculated using eqn (1):[55]

$$\beta = \frac{(m+1)^{\frac{3}{2}}\Delta T(z)}{L_{\text{eff}} I_o} \quad (1)$$

where $L_{\text{eff}} = \frac{(1 - e^{-\alpha L})}{\alpha}$ is the sample length (cm), $\Delta T(z) = 1 - T(z)$ at the focus, $T(z)$ is the transmittance of the sample at z, I_o is the peak on-axis irradiance at the focus (W cm^{-2}), z is the position of the sample corresponding to the focus (cm), $z_o = \frac{\pi\omega_0^2}{\lambda}$ is the Rayleigh range (cm), α is the linear absorption coefficient (cm^{-1}), L is the sample length (cm), ω_0 is the spot size at the focus (cm), and λ is the laser wavelength (cm). Here, m is a constant that characterizes the degree of nonlinearity exhibited by the material and its value can be calculated by fitting eqn (2):[55]

$$T(z) = \sum_{m=0}^{\infty} \frac{[-q(z)]^m}{(m+1)^{\frac{3}{2}}} \quad (2)$$

where $q(z) = \frac{\beta L_{\text{eff}} I_o}{\left(1 + \frac{z^2}{z_o^2}\right)}$. The open aperture curves were fitted using eqn (2) for m = 1 as shown in Fig. 5(a) and (b), which confirms the third order NLO phenomenon. The values of the nonlinear absorption coefficient of the TiO_2 NPs obtained from *M. indica* and *A. indica* are 3.74 × 10^{-12} and 5.15 × 10^{-11}, respectively, which are comparable to the previous results reported by other groups. The value of the nonlinear absorption coefficient depends on several factors such as particles size, experimental conditions and measurement parameters and thus a wide variety of values have been reported in the literature. Furthermore, the nonlinear refractive index values were obtained from the closed aperture curves shown in Fig. 5(c) and (d) using eqn (3)[55] considering the ratio of the incident to the transmitted power at iris to be approximately zero. A valley-peak signature is observed for both the samples, which indicates self-focusing behaviour and a positive value of the nonlinear refractive index. For the calculation of n_2, the contribution of nonlinear refraction through the heat effect is disregarded due to the extremely short pulse duration (approximately 35 fs) in comparison to the thermal rise time.[55]

$$n_2 = \frac{\lambda}{2\pi} \frac{\Delta\varphi}{L_{\text{eff}} I_o} \quad (3)$$

where $\Delta\varphi = \frac{-\Delta T_{pv}}{0.406}$ is the phase change of the transmitted laser beam and $\Delta T_{pv} = T_p - T_v$ is the difference between the peak and the valley transmittance. After putting the values of $\Delta\varphi$ in eqn (3), the values of the nonlinear refractive index are calculated as 2.10 × 10^{-17} and 3.83 × 10^{-17}, respectively, for NPs synthesized using *M. indica and A. indica* (Table 2). Moreover, using the values of the nonlinear absorption coefficient and nonlinear refractive index from eqn (1) and (3), susceptibility ($\chi^{(3)}$) of the material was calculated using eqn (4),[55] which quantifies the material's ability to generate and interact with higher-order optical phenomena.

$$\chi^3 = \chi^3(\text{r}) + i\chi^3(\text{i}) \quad (4)$$

where the real χ^3(r) and imaginary part χ^3(i) are as follows:

$$\chi^3(r) = 10^{-4} \frac{\epsilon_0 c^2 n_0^2 n_2}{\pi} \quad (5)$$

$$\chi^3(i) = 10^{-4} \frac{\epsilon_0 c^2 n_0 \lambda \beta}{4\pi^2} \quad (6)$$

where ϵ_0 is the vacuum permittivity, which represents the permittivity of free space, c represents the speed of light in vacuum, and n_0 represents the refractive index of the material at the fundamental frequency or the linear refractive index. After putting the values of the constants and nonlinear absorption coefficient and refractive index obtained above, the values of susceptibility of real χ^3(r) and imaginary parts χ^3(i) were calculated and provided in Table 2. The values of the third order nonlinear susceptibility are 2.43 × 10^{-15} + i.7.2 × 10^{-18} and 3.91 × 10^{-15} + i.1.06 × 10^{-18}, respectively, for TiO_2 NPs synthesised using *M. indica* and *A. indica*. These values obtained for both the NPs indicate that the materials exhibit a strong nonlinear response to an applied electric field. Also, these NPs possess favourable properties for applications in nonlinear optics, such as frequency conversion, optical switching, and all-optical signal processing.

Table 2 Third-order nonlinear parameters of TiO_2 NPs prepared using *M. indica and A. indica*

Laser parameters: 2.5 mW power, 1 kHz repetition rate and 35 fs frequency				
Sample	Nonlinear absorption coefficient (β) m W^{-1}	Nonlinear refractive index (n_2) m^2 W^{-1}	Real part of susceptibility (χ^3(r))	Imaginary part of susceptibility (χ^3(i))
M. indica	3.74 × 10^{-12}	2.10 × 10^{-17}	2.43 × 10^{-15}	7.2 × 10^{-18}
A. indica	5.15 × 10^{-11}	3.83 × 10^{-17}	3.91 × 10^{-12}	1.06 × 10^{-17}

3.4. Antimicrobial and antioxidant activities

To investigate the antimicrobial activity of TiO_2 NPs synthesized using a green approach against a diverse range of pathogenic organisms, including fungi such as *A. alternata*, *C. gloeosporioides*, *T. harzianum*, and *A. rolfsii*, and the bacterial pathogen *X. oryzae*. To assess the efficacy of the NPs, the agar disk diffusion method was employed at three different concentrations: 60, 80, and 100 μg ml^{-1}. Fig. 6(a) and (b) provides a visual representation of the diameter of the zone of inhibition for both types of NPs tested against *A. alternata* and *C. gloeosporioides*, providing clear evidence of their antimicrobial effectiveness. The obtained ZOI indicates the regions where the growth of the microorganisms is hindered by the presence of the NPs. Furthermore, Fig. 7(a)–(e) clearly depict that upon increasing the concentration of both the NPs (synthesized using *A. indica* and *M. indica*), their corresponding diameters of ZOI increase. This observation suggests that higher NP concentrations lead to a more significant antimicrobial effect. The underlying mechanism behind this phenomenon can be attributed to the gradual release of Ti^{4+} ions from the NP discs into the agar medium during the incubation period. These released ions subsequently interact with the surfaces of fungal cells, inducing damage to their cell walls and membranes.[84] Moreover, the released Ti^{4+} ions can also disrupt the integrity of their cell membranes by binding to sulfur-containing groups, such as cysteine. This interaction triggers oxidative stress within the fungal cells, which ultimately results in an increase in the permeability of the cell membrane. Consequently, the leakage of cellular components occurs, leading to the eventual death of the fungal cells.[46]

The investigation revealed variations in the diameter of the ZOI between the highest and lowest concentrations of NPs, depending on the nature of the fungi and bacteria being tested. For instance, at a concentration of 100 μg ml^{-1}, the NPs synthesized using *A. indica* exhibited a higher ZOI (18.9 ± 0.4 mm) compared to those prepared using *M. indica* (16.3 ± 0.65 mm) against *A. alternata* fungus. However, at the lowest concentration of 60 μg ml^{-1}, the respective ZOIs were 14.2 ± 0.3 mm and 10.3 ± 0.56 mm for NPs synthesized using *A. indica* and *M. indica* against *A. alternata*. Interestingly, the difference in inhibition between the highest and lowest concentrations was greater for NPs synthesized using *M. indica* compared to those synthesized using *A. indica* for *A. alternata* fungus. This trend of inhibition was also observed for other fungi such as *C. gloeosporioides* and *T. harzianum*.

Similarly, for *A. rolfsii*, the ZOIs of NPs synthesized using *A. indica* were 9 ± 0.4 mm and 12 ± 0.7 mm, while for NPs synthesized using *M. indica*, the ZOIs were 12 ± 0.6 mm and 14 ± 0.8 mm at the lowest (60 μg ml^{-1}) and highest concentrations (100 μg ml^{-1}), respectively. In this case, the ZOI was greater for NPs synthesized using *M. indica* compared to those synthesized using *A. indica* at the same concentration. Hence, it can be concluded that both types of NPs exhibited antifungal activity against all the fungi tested, however, NPs prepared using *M. indica* exhibited a somewhat higher antifungal activity than those prepared using *A. indica*. This difference in activity can be attributed to the larger pore diameter observed for the NPs synthesized using *M. indica* compared to those synthesized using *A. indica*, as revealed by the BET analysis (Fig. 3(g) and (h)). A larger pore diameter provides a greater surface area

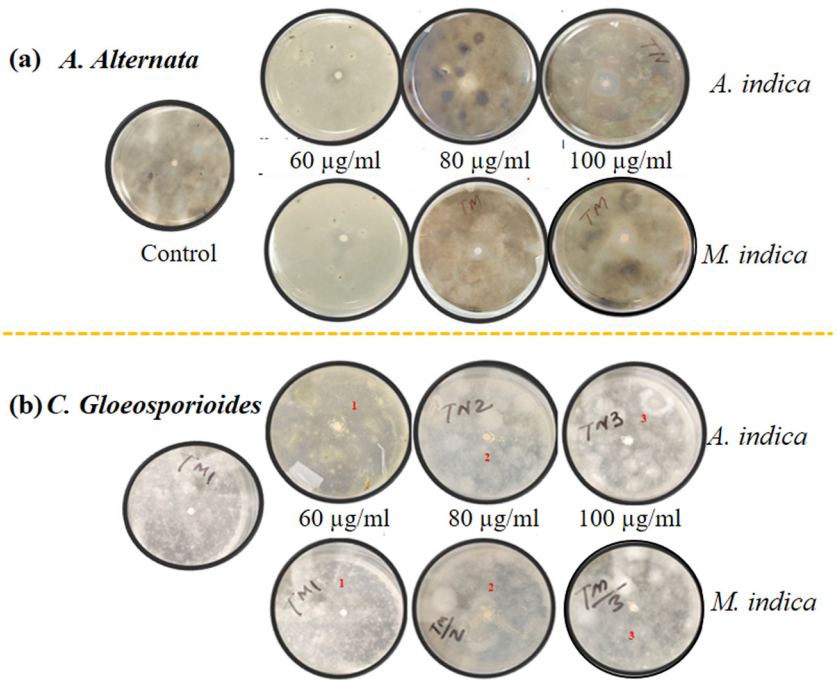

Fig. 6 Evaluation of zone of inhibition of TiO_2 NPs synthesized by *A. indica* and *M. indica* plant extracts against (a) *A. alternata* and (b) *C. gloeosporioides* at 60, 80 and 100 μg ml^{-1} using disk diffusion method.

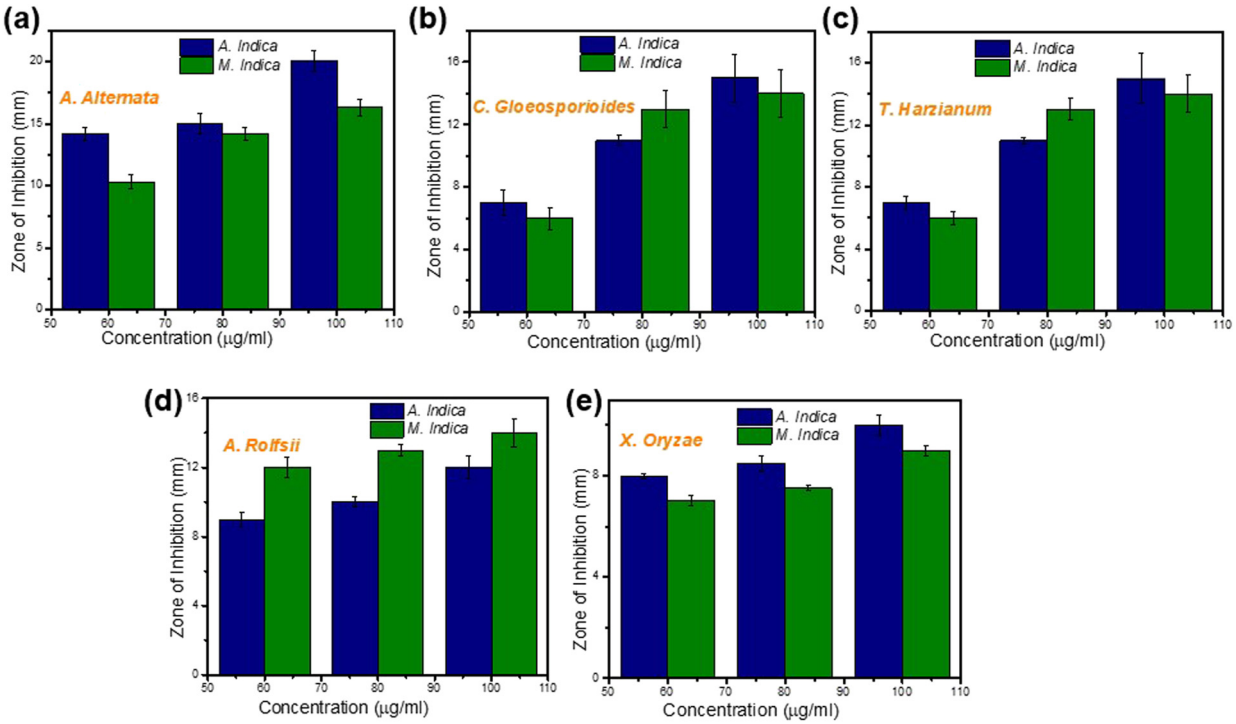

Fig. 7 Antimicrobial activity of green synthesized TiO_2 NPs obtained using *A. indica* and *M. indica* against fungi such as (a) *A. alternata*, (b) *C. gloeosporioides*, (c) *T. harzianum*, and (d) *A. rolfsii*, and the bacterium (e) *X. oryzae* at the concentrations of 60, 80 and 100 μg ml^{-1}.

available for interaction with microbes.[48] This increased surface area allows for more contact between the NPs and microbial cells, thereby enhancing the likelihood of antimicrobial activity.[14] Furthermore, the larger pore diameter of the NPs enables them to accommodate a wider range of microbial cell sizes. This facilitates better penetration of the NPs into microbial cells, leading to increased interaction with the cell membrane and, consequently, higher antimicrobial activity.[50] The plausible mechanism is discussed in detail in the next section 'Mechanism of interaction of fungal cells with NPs'. Additionally, it is worth noting that both types of NPs synthesized using *A. indica* and *M. indica* exhibited equal effectiveness against *X. oryzae*, as illustrated in Fig. 7(e). This intriguing finding suggests that the variation in the structural composition of bacteria, compared to fungi, may contribute to this equal susceptibility. Bacteria possess unique cellular structures and components that may respond differently to the antimicrobial mechanisms employed by the TiO_2 NPs.[84]

Moreover, evaluation of the antioxidant activity of NPs involves the utilization of various methods and assays. A widely employed assay is the DPPH assay, which offers broad applicability for assessing the ability of different antioxidant agents to scavenge free radicals. The scavenging potential of DPPH is associated with the hydrogen or electron-donating activities of antioxidant agents. DPPH is a stable free radical that maintains its structure at room temperature and generates a violet solution when dissolved in methanol.[59] However, in the presence of antioxidant molecules, it undergoes reduction, leading to a colour change in the solution from violet to yellow. The utilization of DPPH offers a convenient and swift method to assess the antioxidant properties of substances.[59] The antioxidant activity of NPs synthesized using *A. indica* and *M. indica* plant extracts was evaluated using the DPPH radical scavenging method, as illustrated in Fig. 8. The results revealed that NPs synthesized using *M. indica* exhibited radical scavenging activities of 34% and 45% at concentrations of 100 and 200 μg ml^{-1} respectively. Conversely, NPs synthesized using *A. indica* demonstrated higher scavenging activities, measuring 38% and 52% at the same concentrations. As a reference standard, ascorbic acid exhibited the highest scavenging activity of 49% and 55% at the concentrations of 100 and 200 μg ml^{-1} respectively. Both types of NPs synthesized using different plant extracts displayed antioxidant activity relative to the standard sample. This can be attributed to the green synthesis approach, which allows for the presence of phytochemicals such as flavonoids and phenolics as capping agents during NP synthesis. Notably, the NPs synthesized using the *A. indica* plant extract exhibited a higher IC_{50} value, indicating better antioxidant activity. This difference can be attributed to variations in the concentration of various phytochemicals present, which facilitate free radical scavenging. It is important to note that the green synthesis approach utilized in this study not only allows for the production of NPs with desirable antioxidant properties, but also highlights the potential of utilizing plant extracts as sustainable resources for NP synthesis. Overall, the DPPH assay revealed the dose-dependent increase in the antioxidant activities of the TiO_2 NPs synthesized using *A. indica* and *M. indica* plant extracts. The results demonstrated the potential of these NPs as effective

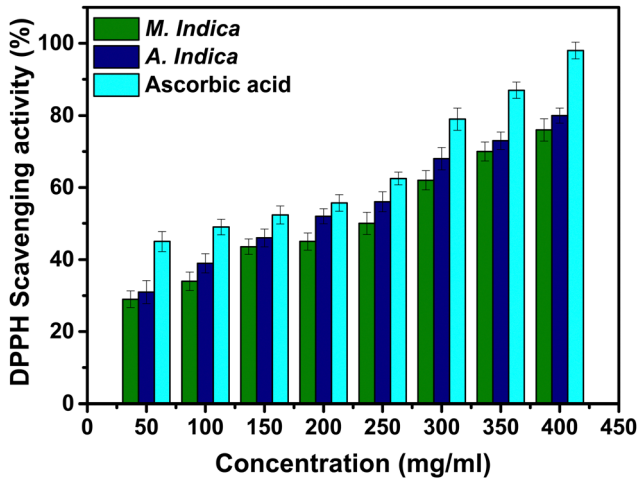

Fig. 8 Free radical scavenging ability of TiO_2 NPs determined using DPPH assay.

radical scavengers, with the NPs synthesized using the *A. indica* extract exhibiting superior antioxidant activity. The findings underscore the importance of green synthesis approaches and highlight the influence of phytochemical concentrations on the antioxidant properties of the synthesized NPs.

3.5. Mechanism of interaction of fungal cells with nanoparticles

Fungal cells, like other eukaryotic cells, possess a well-defined nucleus that contains the genetic material in the form of DNA. Surrounding the nucleus is the cytoplasm, which houses various organelles responsible for different cellular processes. The fungal cell wall is composed of multiple layers, including mannoproteins, β-glucans, and chitin, with the innermost layer serving as a conserved structure onto which the remaining layers are deposited.[39,85] The composition of the cell wall can vary among different fungal species. The fungal cell wall performs several important functions, such as providing rigidity and shape to the cell and facilitating metabolism, ion exchange, and interaction with host defence mechanisms. Glucan, a polysaccharide, is the predominant component of the fungal cell wall. Most glucan polymers are composed of glucose units linked by 1,3 linkages (65–90%), although there are variations with β-1,6, β-1,4, α-1,3, and α-1,4 linkages depending on the fungal species.[86] The β-1,3-D-glucan and chitin molecules form intrachain hydrogen bonds and can assemble into fibrous microfibrils, creating a basket-like scaffold around the cell.[87] β-1,3-D-glucan is responsible for covalently linking other components, making it the critical structural component of the cell wall. Chitin, on the other hand, consists of repeating units of *N*-acetyl glucosamine linked together to form long chains. Chitin acts as a protective barrier, shielding the fungal cell from physical damage and pathogens, while also contributing to cell adhesion and colonization on various substrates. Mannoproteins, a class of glycoproteins, play significant roles in the structure and function of fungal cells. These proteins consist of protein molecules with attached mannose sugars, forming glycosidic linkages. The specific chemical composition of mannoproteins varies among fungal species. Mannoproteins are located on the surface of fungal cells and interact with receptors on host cells, facilitating adhesion, colonization, and the establishment of infections.[88] NPs exhibit antimicrobial activity due to their physicochemical properties. Factors such as size distribution, shape, composition, crystallinity, porosity, agglomeration, and surface charge influence the antifungal activity of NPs.[39] These factors can be manipulated and controlled using various synthesis approaches. In this study, a green synthesis approach was employed to produce NPs, which demonstrated effective antimicrobial properties. The findings are consistent with the existing literature, highlighting the enhanced antimicrobial effects of NPs synthesized through green methods. In addition to the synthesis approach, the surface area of NPs plays a crucial role in determining their antimicrobial efficacy. NPs synthesized using *A. indica* and *M. indica* exhibited surface areas of 94.09 $m^2\ g^{-1}$ and 127.60 $m^2\ g^{-1}$, respectively, as already mentioned above. NPs synthesized using *M. indica*

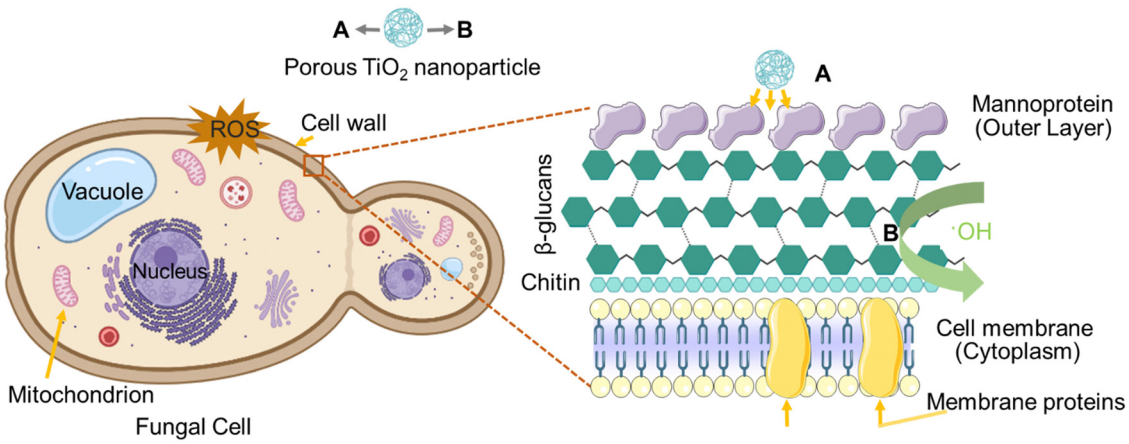

Fig. 9 Mechanism of interaction of porous TiO_2 NPs with the fungal cell at the cellular level involving (A) membrane disruption and (B) ROS generation leading to cell damage (created using https://BioRender.com).

possessed a higher surface area-to-volume ratio compared to those synthesized using *A. indica*, leading to enhanced antimicrobial activity.

There are various plausible mechanisms of interaction of NPs with fungal cells. These mechanisms involve (i) the release of ions by NPs followed by their binding to certain protein groups, affecting their function and interfering with cell permeability, (ii) the increased binding of smaller and higher surface area NPs at various target sites, facilitating diffusion and (iii) the generation of ROS such as hydroxyl radicals, in the vicinity of the fungal cell wall.[85] In the present case, the high surface area TiO_2 NPs synthesized using both plant extracts primarily interact by generating ROS, as discussed in the section on antioxidant activity.[89] As shown in Fig. 9, due to their small size and high surface area, these NPs adhere to the outer layer of the fungal cell wall, which mainly consists of mannoproteins.[90] The interaction between the NPs and the mannoproteins weakens the glycosidic linkages connecting these essential proteins, leading to structural loosening and the disturbance of their function.[91] As a result, the fungal cell wall is disrupted to some extent. Furthermore, the ROS generated by these NPs in the vicinity of the fungal cell wall readily react with the *N*-acetylglucosamine monomer of chitin and/or the glucose monomer of the glucan layers within the fungal cell wall. This reaction results in the cleavage of glycosidic linkages, leading to the rupture of the cell wall.[92] Consequently, the boundaries of the fungal cells are perforated, allowing the passage of intracellular materials.[91] These two synergistic mechanisms ultimately contribute to the cell death of the fungi. The proposed mechanisms align with the existing literature and support the idea that the interaction between TiO_2 NPs and fungal cells results in the disruption and ultimate death of the fungal cells.

4. Conclusion

The present work highlights the potential of green-synthesized TiO_2 NPs as a multifunctional solution for sustainable agriculture. The green synthesis approach, utilizing plant extracts from *A. indica* and *M. indica* as reducing and stabilizing agents, offers numerous advantages. One key benefit is the low toxicity of the resulting NPs, as natural plant extracts replace harsh chemical reagents, ensuring the production of safer NPs for human health and the environment. Furthermore, green synthesis minimizes the production of toxic waste and reduces the environmental impact associated with NP synthesis, aligning with sustainable and eco-friendly practices.

The antimicrobial properties of the TiO_2 NPs synthesized using the green synthesis approach were extensively investigated, revealing their remarkable inhibitory action against a range of pathogenic fungi and bacterial species known to adversely affect crop yield. The effectiveness of these NPs was evaluated using the agar disk-diffusion method, focusing on four fungi (*A. alternata*, *C. gloeosporioides*, *T. harzianum*, and *A. rolfsii*) and one bacterial species (*X. oryzae*). The results demonstrated that both types of NPs exhibited significant antimicrobial efficacy, as evidenced by the formation of inhibition zones. The antimicrobial efficacy of the NPs was observed to be concentration-dependent, with higher concentrations leading to larger zones of inhibition. The antimicrobial activity of the NPs was attributed to their ability to generate ROS, such as hydroxyl radicals, in close proximity to the fungal cell wall. The interaction between the TiO_2 NPs and the fungal cells resulted in the damage of the cell walls and membranes, disrupting their integrity and leading to increased permeability. This, in turn, caused the leakage of cellular components and eventual cell death. Moreover, the NPs showed substantial antioxidant activity, attributed to the presence of phytochemicals like flavonoids and phenolics. Their antioxidant abilities increased with higher doses, indicating their potential as effective antioxidants.

Furthermore, the green-synthesized TiO_2 NPs possess excellent NLO properties. They exhibit high nonlinear absorption coefficients, indicating efficient energy absorption for nonlinear optical processes. The nonlinear absorption coefficient of TiO_2 NPs synthesized using *M. indica* was found to be 3.74×10^{-12}, while for those synthesized using *A. indica*, the value was 5.15×10^{-11}. These values demonstrate the high nonlinear absorption capacity of both types of nanoparticles, indicating their potential for efficient energy absorption and utilization in nonlinear optical processes. Also, the nonlinear refractive indices were calculated to be 2.10×10^{-17} and 3.83×10^{-17} for NPs synthesized using *M. indica* and *A. indica*, respectively. These values signify the materials' ability to exhibit self-focusing behaviour and their response to an applied electric field. The higher value of n_2 obtained for NPs synthesized using *A. indica* suggests enhanced nonlinear optical properties compared to those synthesized using *M. indica*. Additionally, the third-order nonlinear susceptibility values were calculated as $2.43 \times 10^{-15} + i.7.2 \times 10^{-18}$ and $3.91 \times 10^{-15} + i.1.06 \times 10^{-18}$ for TiO_2 NPs synthesized using *M. indica* and *A. indica*, respectively. These values further confirm the strong nonlinear response of the NPs to an applied electric field and emphasize their suitability for application in nonlinear optics. These quantitative measurements provide evidence for the potential applications of TiO_2 NPs in nonlinear optical processes, such as frequency conversion, biosensors, optical switching, and all-optical signal processing. The study contributes valuable insights into the feasibility and efficacy of these NPs for a broad range of technological applications.

Combining their antimicrobial activity, antioxidant properties, and strong nonlinear optical characteristics, the green-synthesized TiO_2 NPs hold great promise in addressing critical challenges in sustainable agriculture. Their multifunctional nature opens avenues for the development of novel antimicrobial agents, biosensors, and nanomaterial-based strategies for crop protection, ultimately contributing to improved crop quality, yield, and resource management. The green synthesis approach provides a sustainable and environmentally friendly method for producing NPs with desirable properties, paving the way for greener agricultural practices and enhanced food security.

Data availability statement

Raw data were generated at the National Physical Laboratory and Indian Institute of Agricultural Sciences, Pusa road, New Delhi. All data are presented in the article.

Author contributions

Archana Rana: conceptualization, writing – original draft, methodology, investigation; Saurabh Pathak: formal analysis, supervision, writing – reviewing and editing; Kapil Kumar, Anjali Kumari, Samridhi Chopra: formal analysis, investigation; Ritu Srivastava, Mahesh Kumar: resources, validation, writing – reviewing and editing; Deeba Kamil: resources, software; Sang-Koog Kim: supervision, writing – reviewing and editing; and Rajni Verma, Shailesh Narain Sharma: supervision, validation, conceptualization, writing – reviewing and editing.

Conflicts of interest

There are no conflicts to declare.

Acknowledgements

The author Archana Rana would like to acknowledge the AcSIR for providing necessary facilities to carry out the experimental work and also thank the University Grants Commission (UGC-90802) for providing the Research Fellowship.

References

1 A. Spanos, K. Athanasiou, A. Ioannou, V. Fotopoulos and T. Krasia-Christoforou, Functionalized Magnetic Nanomaterials in Agricultural Applications, *Nanomaterials*, 2021, **11**, 3106.
2 L. R. Khot, S. Sankaran, J. M. Maja, R. Ehsani and E. W. Schuster, Applications of nanomaterials in agricultural production and crop protection: A review, *Crop Prot.*, 2012, **35**, 64–70.
3 N. Chaudhry, S. Dwivedi, V. Chaudhry, A. Singh, Q. Saquib, A. Azam and J. Musarrat, Bio-inspired nanomaterials in agriculture and food: Current status, foreseen applications and challenges, *Microb. Pathog.*, 2018, **123**, 196–200.
4 A. Ioannou, G. Gohari, P. Papaphilippou, S. Panahirad, A. Akbari, M. R. Dadpour, T. Krasia-Christoforou and V. Fotopoulos, Advanced nanomaterials in agriculture under a changing climate: the way to the future?, *Environ. Exp. Bot.*, 2020, **176**, 104048.
5 A. Rani, K. Rani, J. Tokas, Anamika, A. Singh, R. Kumar, H. Punia and S. Kumar, Nanomaterials for agriculture input use efficiency, *Resour. Use Effic. agric.*, 2020, 137–175.
6 N. Chakraborty, S. Gandhi, R. Verma and I. Roy, Emerging Prospects of Nanozymes for Antibacterial and Anticancer Applications, *Biomedicines*, 2022, **10**, 1378.
7 P. Sánchez, A. Vélez-del-Burgo, E. Suñén, J. Martínez and I. Postigo, Fungal allergen and mold allergy diagnosis: Role and relevance of Alternaria alternata Alt a 1 protein family, *J. Fungi*, 2022, **8**, 277.
8 N. Chakraborty, K. Mukherjee, A. Sarkar and K. Acharya, Interaction between bean and Colletotrichum gloeosporioides: understanding through a biochemical approach, *Plants*, 2019, **8**, 345.
9 T. Yang, T. Zhang, X. Zhou, P. Wang, J. Gan, B. Song, S. Yang and C.-G. Yang, Dysregulation of ClpP by small-molecule activators used against Xanthomonas oryzae pv. oryzae infections, *J. Agric. Food Chem.*, 2021, **69**, 7545–7553.
10 T. D. Majumdar, M. Singh, M. Thapa, M. Dutta, A. Mukherjee and C. K. Ghosh, Size-dependent antibacterial activity of copper nanoparticles against Xanthomonas oryzae pv. oryzae–A synthetic and mechanistic approach, Colloid and Interface Science, *Communications*, 2019, **32**, 100190.
11 S. Mücke, M. Reschke, A. Erkes, C.-A. Schwietzer, S. Becker, J. Streubel, R. D. Morgan, G. G. Wilson, J. Grau and J. Boch, Transcriptional reprogramming of rice cells by Xanthomonas oryzae TALEs, *Front. Plant Sci.*, 2019, **10**, 162.
12 L. Goswami, N. Aggarwal, M. Singh, R. Verma, P. Vashishtha, S. K. Jain, J. Tawale, R. Pandey and G. Gupta, GaN Nanotowers Grown on Si (111) and Functionalized with Au Nanoparticles and ZnO Nanorods for Highly Responsive UV Photodetectors, *ACS Appl. Nano Mater.*, 2020, **3**, 8104–8116.
13 M. Kumar, S. Rani, R. Parmar, M. Amati, L. Gregoratti, A. Ghosh, S. Pathak, A. Kumar, X. Wang and V. N. Singh, The ultra-high thermoelectric power factor in facile and scalable single-step thermal evaporation fabricated composite SnSe/Bi thin films, *J. Mater. Chem. C*, 2022, **10**, 18017–18024.
14 A. K. Srivastava, J. S. Tawale, R. Verma, D. Agarwal, C. Sharma, A. Kumar and M. K. Gupta, Morphological evolution driven semiconducting nanostructures for emerging solar, biological and nanogenerator applications, *Mater. Adv.*, 2022, **3**, 8030–8062.
15 S. Pathak, R. Zhang, B. Gayen, V. Kumar, H. Zhang, R. P. Pant and X. Wang, Ultra-low friction self-levitating nanomagnetic fluid bearing for highly efficient wind energy harvesting, *Sustainable Energy Technol. Assess.*, 2022, **52**, 102024.
16 S. Pathak, R. Zhang, K. Bun, H. Zhang, B. Gayen and X. Wang, Development of a novel wind to electrical energy converter of passive ferrofluid levitation through its parameter modelling and optimization, *Sustainable Energy Technol. Assess.*, 2021, **48**, 101641.
17 S. Pathak, K. Jain, Noorjahan, V. Kumar and R. P. Pant, Magnetic Fluid Based High Precision Temperature Sensor, *IEEE Sens. J.*, 2017, **17**, 2670–2675.
18 P. Devi, R. Verma and J. P. Singh, Advancement in electrochemical, photocatalytic, and photoelectrochemical CO_2 reduction: Recent progress in the role of oxygen vacancies in catalyst design, *J. CO_2 Util.*, 2022, **65**, 102211.
19 S. Pathak, R. Verma, S. Singhal, R. Chaturvedi, P. Kumar, P. Sharma, R. P. Pant and X. Wang, Spin dynamics investigations of multifunctional ambient scalable Fe_3O_4 surface

decorated ZnO magnetic nanocomposite using FMR, *Sci. Rep.*, 2021, **11**, 3799.
20 R. Verma and N. Mahmood, Bioinspired synthesis of inorganic nanomaterials, *Green Sustainable Process for Chemical and Environmental Engineering and Science*, Elsevier, 2021, pp. 171–200.
21 R. Maria-Hormigos, C. C. Mayorga-Martinez and M. Pumera, Magnetic Hydrogel Microrobots as Insecticide Carriers for In Vivo Insect Pest Control in Plants, *Small*, 2022, 2204887.
22 J. Li, A. Khalid, R. Verma, A. Abraham, F. Qazi, X. Dong, G. Liang and S. Tomljenovic-Hanic, Silk Fibroin Coated Magnesium Oxide Nanospheres: A Biocompatible and Biodegradable Tool for Noninvasive Bioimaging Applications, *Nanomaterials*, 2021, **11**, 695.
23 R. Verma, S. Pathak, A. K. Srivastava, S. Prawer and S. Tomljenovic-Hanic, ZnO nanomaterials: Green synthesis, toxicity evaluation and new insights in biomedical applications, *J. Alloys Compd.*, 2021, **876**, 160175.
24 A. Ditta and M. Arshad, Applications and perspectives of using nanomaterials for sustainable plant nutrition, *Nanotechnol. Rev.*, 2016, **5**, 209–229.
25 A. Gogos, K. Knauer and T. D. Bucheli, Nanomaterials in plant protection and fertilization: current state, foreseen applications, and research priorities, *J. Agric. Food Chem.*, 2012, **60**, 9781–9792.
26 R. Verma, J. Gangwar and A. K. Srivastava, Multiphase TiO_2 nanostructures: a review of efficient synthesis, growth mechanism, probing capabilities, and applications in biosafety and health, *RSC Adv.*, 2017, **7**, 44199–44224.
27 R. Verma, S. Singh, M. K. Dalai, M. Saravanan, V. V. Agrawal and A. K. Srivastava, Photocatalytic degradation of polypropylene film using TiO_2-based nanomaterials under solar irradiation, *Mater. Des.*, 2017, **133**, 10–18.
28 R. Verma, A. Awasthi, P. Singh, R. Srivastava, H. Sheng, J. Wen, D. J. Miller and A. K. Srivastava, Interactions of titania based nanoparticles with silica and green-tea: Photodegradation and -luminescence, *J. Colloid Interface Sci.*, 2016, **475**, 82–95.
29 R. Verma, V. B. Chaudhary, L. Nain and A. K. Srivastava, Antibacterial characteristics of TiO_2 nano-objects and their interaction with biofilm, *Mater. Technol.*, 2017, **32**, 385–390.
30 D. Banerjee, S. S. B. Moram, C. Byram, J. Rathod, T. Jena, G. K. Podagatlapalli and V. R. Soma, Plasmon-enhanced ultrafast and tunable thermo-optic nonlinear optical properties of femtosecond laser ablated TiO_2 and Silver-doped TiO_2 nanoparticles, *Appl. Surf. Sci.*, 2021, **569**, 151070.
31 S. Gbadamasi, M. Mohiuddin, V. Krishnamurthi, R. Verma, M. W. Khan, S. Pathak, K. Kalantar-Zadeh and N. Mahmood, Interface chemistry of two-dimensional heterostructures – fundamentals to applications, *Chem. Soc. Rev.*, 2021, **50**, 4684–4729.
32 R. Viter, A. Tereshchenko, V. Smyntyna, J. Ogorodniichuk, N. Starodub, R. Yakimova, V. Khranovskyy and A. Ramanavicius, Toward development of optical biosensors based on photoluminescence of TiO_2 nanoparticles for the detection of Salmonella, *Sens. Actuators, B*, 2017, **252**, 95–102.
33 P. K. Rai, V. Kumar, S. Lee, N. Raza, K.-H. Kim, Y. S. Ok and D. C. Tsang, Nanoparticle-plant interaction: Implications in energy, environment, and agriculture, *Environ. Int.*, 2018, **119**, 1–19.
34 A. Maholiya, P. Ranjan, R. Khan, S. Murali, R. C. Nainwal, P. S. Chauhan, N. Sathish, J. Chourasia and A. K. Srivastava, An Insight into the Role of Carbon Dots in Agriculture System: A Review, *Environ. Sci.: Nano*, 2023, **10**, 959–995.
35 M. Trejo-Valdez, R. Torres-Martínez, N. Peréa-López, P. Santiago-Jacinto and C. Torres-Torres, Contribution of the Two-Photon Absorption to the Third Order Nonlinearity of Au Nanoparticles Embedded in TiO_2 Films and in Ethanol Suspension, *J. Phys. Chem. C*, 2010, **114**, 10108–10113.
36 L. Dong, H. Chu, X. Wang, Y. Li, S. Zhao and D. Li, Enhanced broadband nonlinear optical response of TiO_2/CuO nanosheets via oxygen vacancy engineering, *Nanophotonics*, 2021, **10**, 1541–1551.
37 J.-H. Lee, B. Kim, Y. Kim and S.-K. Kim, Ultra-high rate of temperature increment from superparamagnetic nanoparticles for highly efficient hyperthermia, *Sci. Rep.*, 2021, **11**, 4969.
38 D. Devipriya and S. M. Roopan, Cissus quadrangularis mediated ecofriendly synthesis of copper oxide nanoparticles and its antifungal studies against Aspergillus niger, Aspergillus flavus, *Mater. Sci. Eng., C*, 2017, **80**, 38–44.
39 A. Rana, S. Pathak, D.-K. Lim, S.-K. Kim, R. Srivastava, S. N. Sharma and R. Verma, Recent Advancements in Plant- and Microbe-Mediated Synthesis of Metal and Metal Oxide Nanomaterials and Their Emerging Antimicrobial Applications, *ACS Appl. Nano Mater.*, 2023, **6**, 8106–8134.
40 R. Singh, S. Pathak, K. Jain, Noorjahan and S.-K. Kim, Correlating the Dipolar Interactions Induced Magneto-Viscoelasticity and Thermal Conductivity Enhancements in Nanomagnetic Fluids, *Small*, 2023, 2205741.
41 S. Pathak, R. Verma, P. Kumar, A. Singh, S. Singhal, P. Sharma, K. Jain, R. P. Pant and X. Wang, Facile Synthesis, Static, and Dynamic Magnetic Characteristics of Varying Size Double-Surfactant-Coated Mesoscopic Magnetic Nanoparticles Dispersed Stable Aqueous Magnetic Fluids, *Nanomaterials*, 2021, **11**, 3009.
42 J.-H. Lee, Y. Kim and S.-K. Kim, Highly efficient heat-dissipation power driven by ferromagnetic resonance in MFe_2O_4 (M = Fe, Mn, Ni) ferrite nanoparticles, *Sci. Rep.*, 2022, **12**, 5232.
43 T. V. Surendra and S. M. Roopan, Photocatalytic and antibacterial properties of phytosynthesized CeO_2 NPs using Moringa oleifera peel extract, *J. Photochem. Photobiol., B*, 2016, **161**, 122–128.
44 D. Titus, E. J. Samuel and S. Roopan, Green Synthesis, Characterization and Applications of Nanoparticles, *Micro Nanotechnol.*, 2019, **12**, 303–319.
45 M. Joy, G. Chandrasekharan, M. A. Khan, M. Arunachalapandi, T. Chellapandi, D. Harish, D. Chitra and S. M. Roopan, Citrus lemon mediated green synthesis of

ZnTiO3 nanospheres for the degradation of petrochemical wastewater, *Environ. Qual. Manage.*, 2022, **32**, 159–169.

46 A. Ansari, V. U. Siddiqui, W. U. Rehman, M. K. Akram, W. A. Siddiqi, A. M. Alosaimi, M. A. Hussein and M. Rafatullah, Green Synthesis of TiO_2 Nanoparticles Using Acorus calamus Leaf Extract and Evaluating Its Photocatalytic and In Vitro Antimicrobial Activity, *Catalysts*, 2022, **12**, 181.

47 D. Achudhan, S. Vijayakumar, B. Malaikozhundan, M. Divya, M. Jothirajan, K. Subbian, Z. I. González-Sánchez, S. Mahboob, K. A. Al-Ghanim and B. Vaseeharan, The antibacterial, antibiofilm, antifogging and mosquitocidal activities of titanium dioxide (TiO_2) nanoparticles green-synthesized using multiple plants extracts, *J. Environ. Chem. Eng.*, 2020, **8**, 104521.

48 S. M. Roopan, R. S. Mathew, S. S. Mahesh, D. Titus, K. Aggarwal, N. Bhatia, K. I. Damodharan, K. Elumalai and J. J. Samuel, Environmental friendly synthesis of zinc oxide nanoparticles and estimation of its larvicidal activity against Aedes aegypti, *Int. J. Environ. Sci. Technol.*, 2019, **16**, 8053–8060.

49 V. Helan, J. J. Prince, N. A. Al-Dhabi, M. V. Arasu, A. Ayeshamariam, G. Madhumitha, S. M. Roopan and M. Jayachandran, Neem leaves mediated preparation of NiO nanoparticles and its magnetization, coercivity and antibacterial analysis, *Results Phys.*, 2016, **6**, 712–718.

50 W. Ahmad, K. K. Jaiswal and S. Soni, Green synthesis of titanium dioxide (TiO_2) nanoparticles by using Mentha arvensis leaves extract and its antimicrobial properties, *Inorg. Nano-Metal Chem.*, 2020, **50**, 1032–1038.

51 P. Kumar, S. Pathak, K. Jain, A. Singh, Kuldeep, G. A. Basheed and R. P. Pant, Low-temperature large-scale hydrothermal synthesis of optically active PEG-200 capped single domain $MnFe_2O_4$ nanoparticles, *J. Alloys Compd.*, 2022, **904**, 163992.

52 R. Verma, B. Mantri and A. Kumar Srivastava, Shape Control Synthesis, Characterizations, Mechanisms And Optical Properties Of Larg Scaled Metal oxide Nanostructures Of ZnO And TiO_2, Advanced, *Mater. Lett.*, 2015, **6**, 324–333.

53 R. Verma, K. K. Naik, J. Gangwar and A. K. Srivastava, Morphology, mechanism and optical properties of nanometer-sized MgO synthesized via facile wet chemical method, *Mater. Chem. Phys.*, 2014, **148**, 1064–1070.

54 P. Kumar, S. Pathak, A. Singh, Kuldeep, H. Khanduri, X. Wang, G. A. Basheed and R. P. Pant, Optimization of cobalt concentration for improved magnetic characteristics and stability of CoxFe3-xO4 mixed ferrite nanomagnetic fluids, *Mater. Chem. Phys.*, 2021, 124476.

55 M. Vij, Sonia, H. Yadav, N. Vashistha, P. Kumar and K. K. Maurya, Crystal growth, structure and Z-scan studies of novel diisopropylammonium nicotinate crystal, *J. Mol. Struct.*, 2020, **1206**, 127759.

56 F. Paraguay-Delgado, L. Hermida-Montero, J. Morales-Mendoza, Z. Durán-Barradas, A. I. Mtz-Enriquez and N. Pariona, Photocatalytic properties of Cu-containing ZnO nanoparticles and their antifungal activity against agriculture-pathogenic fungus, *RSC Adv.*, 2022, **12**, 9898–9908.

57 S. M. Roopan, D. D. Priya, S. Shanavas, N. A. Al-Dhabi and M. V. Arasu, CuO/C nanocomposite: Synthesis and optimization using sucrose as carbon source and its antifungal activity, *Mater. Sci. Eng., C*, 2019, **101**, 404–414.

58 C. Perez, Antibiotic assay by agar-well diffusion method, *Acta Biol. Med. Exp.*, 1990, **15**, 113–115.

59 G. Marinova and V. Batchvarov, Evaluation of the methods for determination of the free radical scavenging activity by DPPH, Bulgarian, *J. Agric. Sci.*, 2011, **17**, 11–24.

60 S. Baliyan, R. Mukherjee, A. Priyadarshini, A. Vibhuti, A. Gupta, R. P. Pandey and C.-M. Chang, Determination of Antioxidants by DPPH Radical Scavenging Activity and Quantitative Phytochemical Analysis of Ficus religiosa, *Molecules*, 2022, **27**, 1326.

61 P. Kumar, S. Pathak, A. Singh, K. Jain, H. Khanduri, L. Wang, S.-K. Kim and R. P. Pant, Observation of intrinsic fluorescence in cobalt ferrite magnetic nanoparticles by Mn^{2+} substitution and tuning the spin dynamics by cation distribution, *J. Mater. Chem. C*, 2022, **10**, 12652–12679.

62 B. Choudhury and A. Choudhury, Luminescence characteristics of cobalt doped TiO_2 nanoparticles, *J. Lumin.*, 2012, **132**, 178–184.

63 R. Li, Y. Gan, Q. L. Song, Z. H. Zhu, J. Shi, H. Yang, W. Wang, P. Chen and C. M. Li, Bidirectional mediation of TiO_2 nanowires field effect transistor by dipole moment from purple membrane, *Nanoscale*, 2010, **2**, 1474–1479.

64 P. Kumar, S. Pathak, A. Singh, H. Khanduri, K. Jain, J. Tawale, L. Wang, G. Basheed and R. Pant, Enhanced static and dynamic magnetic properties of PEG-400 coated $CoFe_{2-x}Er_xO_4$ ($0.7 \leq x \leq 0$) nanoferrites, *J. Alloys Compd.*, 2021, **887**, 161418.

65 P. Kumar, S. Pathak, A. Singh, K. Jain, H. Khanduri, L. Wang, J. Partridge and R. Pant, Effect of post annealing process on structural, magnetic and spin dynamics properties of $MnFe_2O_4$ nanoparticles, *Mater. Today: Proc.*, 2023, DOI: **10.1016/j.matpr.2023.05.456**.

66 A. Singh, S. Pathak, P. Kumar, P. Sharma, A. Rathi, G. A. Basheed, K. K. Maurya and R. P. Pant, Tuning the magnetocrystalline anisotropy and spin dynamics in $Co_xZn_{1-x}Fe_2O_4$ ($0 \leq x \leq 1$) nanoferrites, *J. Magn. Magn. Mater.*, 2020, **493**, 165737.

67 S. Pathak, K. Jain, P. Kumar, X. Wang and R. P. Pant, Improved thermal performance of annular fin-shell tube storage system using magnetic fluid, *Appl. Energy*, 2019, **239**, 1524–1535.

68 P. Kumar, H. Khanduri, S. Pathak, A. Singh, G. A. Basheed and R. P. Pant, Temperature selectivity for single phase hydrothermal synthesis of PEG-400 coated magnetite nanoparticles, *Dalton Trans.*, 2020, **49**, 8672–8683.

69 A. Singh, P. Kumar, S. Pathak, K. Jain, P. Garg, M. Pant, A. K. Mahapatro, D. Rath, L. Wang, S.-K. Kim, K. K. Maurya and R. P. Pant, A threefold increase in SAR performance for magnetic hyperthermia by compositional tuning in zinc-substituted iron oxide superparamagnetic nanoparticles with superior biocompatibility, *J. Alloys Compd.*, 2023, **968**, 171868.

70 S. Adesoye and K. Dellinger, ZnO and TiO_2 nanostructures for surface-enhanced Raman scattering-based biosensing: A review, *Sens. Bio-Sens. Res.*, 2022, 100499.
71 M. Khairy, E. Kamar and M. Mousa, Photocatalytic activity of nano-sized Ag and Au metal-doped TiO_2 embedded in rGO under visible light irradiation, *Mater. Sci. Eng., B*, 2022, **286**, 116023.
72 P. Praveen, G. Viruthagiri, S. Mugundan and N. Shanmugam, Structural, optical and morphological analyses of pristine titanium di-oxide nanoparticles-Synthesized via sol-gel route, *Spectrochim. Acta, Part A*, 2013, **117**, 622–629.
73 P. Kumar, S. Pathak, A. Singh, H. Khanduri, G. A. Basheed, L. Wang and R. P. Pant, Microwave spin resonance investigation on the effect of post processing annealing of $CoFe_2O_4$ nanoparticles, *Nanoscale Adv.*, 2020, **2**, 1939–1948.
74 R. Verma, S. Pathak, K. K. Dey, S. Sikarwar, B. C. Yadav and A. K. Srivastava, Facile synthesized zinc oxide nanorod film humidity sensor based on variation in optical transmissivity, *Nanoscale Adv.*, 2022, **4**, 2902–2912.
75 N. Marwaha, B. K. Gupta, R. Verma and A. K. Srivastava, Facile synthesis and characterization of pH-dependent pristine MgO nanostructures for visible light emission, *J. Mater. Sci.*, 2017, **52**, 10480–10484.
76 N. Jain, N. Marwaha, R. Verma, B. K. Gupta and A. K. Srivastava, Facile synthesis of defect-induced highly-luminescent pristine MgO nanostructures for promising solid-state lighting applications, *RSC Adv.*, 2016, **6**, 4960–4968.
77 L. Goswami, N. Aggarwal, R. Verma, S. Bishnoi, S. Husale, R. Pandey and G. Gupta, Graphene Quantum Dot-Sensitized ZnO-Nanorod/GaN-Nanotower Heterostructure-Based High-Performance UV Photodetectors, *ACS Appl. Mater. Interfaces*, 2020, **12**, 47038–47047.
78 R. Verma, S. Pyreddy, C. E. Redmond, F. Qazi, A. Khalid, N. M. O'Brien-Simpson, R. Shukla and S. Tomljenovic-Hanic, Detection and identification of amino acids and proteins using their intrinsic fluorescence in the visible light spectrum, *Anal. Chim. Acta*, 2023, **1282**, 341925.
79 A. Rana, A. K. Chaudhary, S. Saini, R. Srivastava, M. Kumar and S. N. Sharma, Ultrafast transient absorption spectroscopic (UFTAS) and antibacterial efficacy studies of phytofabricated silver nanoparticles using Ocimum Sanctum leaf extract, *Inorg. Chem. Commun.*, 2023, **147**, 110233.
80 P. Sharma, V. V. Alekhya, S. Pathak, K. Jain, P. Tomar, G. A. Basheed, K. K. Maurya and R. P. Pant, A novel experimental approach for direct observation of magnetic field induced structuration in ferrofluid, *J. Magn. Magn. Mater.*, 2021, 168024.
81 B. Sivasankari and S. M. Roopan, L-Malic acid-doped Guanidinium Carbonate crystal: A New NLO Material and its photoluminescence study, *Optik*, 2021, **226**, 165909.
82 V. Crasta, N. B. Rithin Kumar, K. Rajesh, R. Bairy and P. S. Patil, Promising PVA/TiO_2, CuO filled nanocomposites for electrical and third order nonlinear optical applications, *Opt. Mater.*, 2019, **95**, 109218.
83 X. Yu, B. Ding, H. Lu, Y. Huo, Q. Peng, X. Xiu, C. Zhang, C. Yang, S. Jiang and B. Man, Third-order optical nonlinearity in nonstoichiometric amorphous silicon carbide films, *J. Alloys Compd.*, 2019, **794**, 518–524.
84 K. H. Ibrahem, F. A. Ali and S. M. A. Sorchee, Biosynthesis and characterization with antimicrobial activity of TiO_2 nanoparticles using probiotic Bifidobacterium bifidum, *Cell. Mol. Biol.*, 2020, **66**, 111–117.
85 J. A. Kumar, T. Krithiga, S. Manigandan, S. Sathish, A. A. Renita, P. Prakash, B. N. Prasad, T. P. Kumar, M. Rajasimman and A. Hosseini-Bandegharaei, A focus to green synthesis of metal/metal based oxide nanoparticles: Various mechanisms and applications towards ecological approach, *J. Cleaner Prod.*, 2021, **324**, 129198.
86 D. Pérez-Mendoza, L. Romero-Jiménez, M. Á. Rodríguez-Carvajal, M. J. Lorite, S. Muñoz, A. Olmedilla and J. Sanjuán, The Role of Two Linear β-Glucans Activated by c-di-GMP in Rhizobium etli CFN42, *Biology*, 2022, **11**, 1364.
87 N. A. Gow, J.-P. Latge and C. A. Munro, The fungal cell wall: structure, biosynthesis, and function, *Microbiol. Spectrum*, 2017, **5**(3), 01.
88 A. Rivera, J. Lodge and C. Xue, Harnessing the immune response to fungal pathogens for vaccine development, *Annu. Rev. Microbiol.*, 2022, **76**, 703–726.
89 Y. Li, P. Zhang, M. Li, N. Shakoor, M. Adeel, P. Zhou, M. Guo, Y. Jiang, W. Zhao and B. Lou, Application and mechanisms of metal-based nanoparticles in the control of bacterial and fungal crop diseases, *Pest Manage. Sci.*, 2023, **79**, 21–36.
90 S. Gangadoo, C. Xu, D. Cozzolino, K. Latham, E. Della Gaspera, J. Chapman and V. K. Truong, Probing nanoscale interactions of antimicrobial zinc oxide quantum dots on bacterial and fungal cell surfaces, *Adv. Mater. Interfaces*, 2022, **9**, 2101484.
91 K. Mukherjee, K. Acharya, A. Biswas and N. R. Jana, TiO_2 nanoparticles co-doped with nitrogen and fluorine as visible-light-activated antifungal agents, *ACS Appl. Nano Mater.*, 2020, **3**, 2016–2025.
92 Y. N. Slavin and H. Bach, Mechanisms of Antifungal Properties of Metal Nanoparticles, *Nanomaterials*, 2022, **12**, 4470.